Mississippi State University
Scholars Junction

Theses and Dissertations | Theses and Dissertations

8-9-2019

Application of Raman and fluorescence spectroscopy to detect changes in the chemical profile of water subject to polarization, vegetation under stress, and murine blood components

Supriya Nagpal

Follow this and additional works at: https://scholarsjunction.msstate.edu/td

Recommended Citation
Nagpal, Supriya, "Application of Raman and fluorescence spectroscopy to detect changes in the chemical profile of water subject to polarization, vegetation under stress, and murine blood components" (2019). *Theses and Dissertations*. 713.
https://scholarsjunction.msstate.edu/td/713

This Graduate Thesis - Open Access is brought to you for free and open access by the Theses and Dissertations at Scholars Junction. It has been accepted for inclusion in Theses and Dissertations by an authorized administrator of Scholars Junction. For more information, please contact scholcomm@msstate.libanswers.com.

www.manaraa.com

Application of Raman and fluorescence spectroscopy to detect changes in the chemical profile of water subject to polarization, vegetation under stress, and murine blood components

By

Supriya Nagpal

A Thesis
Submitted to the Faculty of
Mississippi State University
in Partial Fulfillment of the Requirements
for the Degree of Master of Science
in Physics
in the Department of Physics and Astronomy

Mississippi State, Mississippi

August 2019

www.manaraa.com

Copyright by

Supriya Nagpal

2019

www.manaraa.com

Application of Raman and fluorescence spectroscopy to detect changes in the chemical profile of water subject to polarization, vegetation under stress, and murine blood components

By

Supriya Nagpal

Approved:

_____

Gombojav O. Ariunbold
(Major Professor)

_____

Prabhakar Pradhan
(Committee Member)

_____

Hendrik F. Arnoldus
(Committee Member/ Graduate Coordinator)

_____

Rick Travis
Dean
College of Arts & Sciences

www.manaraa.com

Name: Supriya Nagpal

Date of Degree: August 9, 2019

Institution: Mississippi State University

Major Field: Physics

Major Professor: Gombojav O. Ariunbold

Title of Study: Application of Raman and fluorescence spectroscopy to detect changes in the chemical profile of water subject to polarization, vegetation under stress, and murine blood components

Pages in Study: 69

Candidate for Degree of Master of Science

This thesis broadly describes the construction of two kinds of spectroscopic set-ups to analyze properties of various materials. In the first part, construction of a Raman spectrometer and a high-throughput *in-vivo* detection for early plant abiotic stress responses is described. Following which, the set-up is modified into a microscope employed to study Murine blood components with samples varying in age. Initial Raman set-up is also improvised using a polarizer in order to gain deeper understanding of the vibrational and rotational bonds in water.

The second part of the thesis explains the construction of a laser-induced fluorescence (LIF) sensor module. Performance testing and experiments were carried out with the sensor module to monitor stress in vegetation and fruits and also detect toxins found in corn and carcinogenic compounds in gasoline. The module was further mounted to an unmanned aerial vehicle for field surveys and preliminary testing in flight is described.

www.manaraa.com

ACKNOWLEDGEMENTS

Firstly, I would like to thank my thesis advisor, Dr. Gombojav of Physics and Astronomy Department at Mississippi State University (MSU) for providing me with the opportunity to work with him in his laboratory. I would also like to thank Dr. Arnoldus, our graduate coordinator for supporting me and steering me in the right direction whenever he thought I needed it.

I would also like to thank Dr. Li in Plant Physiology department (MSU) for providing the plants, Dr. Dash in Geosciences department (MSU) for providing DI water and storing our mice samples and Dr. Gary Windham, Dr. William P. William and Dr. Mathew Boo in USDA (otherwise teaching in MSU) for their support in survey and flying the quadcopter in North farm. Thanks for the support from University of Tennessee Health Science Center (UTHSC) laboratory as well for proving the mice blood samples. Besides that, I would like to thank my lab mates for working with me and former students, Adam Powers and Shane Clark for helping me with some projects.

Lastly, I would like to dedicate this work to my parents, Mr. Dev Nagpal and Dr. Swati Nagpal, who tirelessly helped and guided me through my endeavors at MSU.

www.manaraa.com

TABLE OF CONTENTS

www.manaraa.com

www.manaraa.com

LIST OF TABLES

www.manaraa.com

LIST OF FIGURES

www.manaraa.com

www.manaraa.com

www.manaraa.com

www.manaraa.com

LIST OF ACRONYMS

EMCCD - Electron Multiplied Charged Couple Device

IR - Infrared

PCA - Principal Components Analysis

PC - Principal Component

DI - Deionized

FWHM - Full Width at Half Maxima

PMT - Photo Multiplier Tube

NMR - Nuclear Magnetic Resonance

ROS - Reactive Oxygen Species

RI - Recombinant Inbred

RS - Raman Spectroscopy

LIF - Laser-Induced Fluorescence

UV - Ultraviolet

F690 - Red Chlorophyll Fluorescence

F740 - Far Red Chlorophyll Fluorescence

BGY - Bright Greenish Yellow

PAH - Polycyclic Aromatic Hydrocarbons

UAV - Unmanned Aerial Vehicle

UAS - Unmanned Aerial System

www.manaraa.com

SD - Secure Digital

TFT - Thin Film Transistor

RPi- Raspberry Pi

EOL - End of Line

GUI - Graphical User Interface

I/O - Input/output

AMP - Aviation Maintenance Practice

GPS - Global Positioning System

LED - Light Emitting Diode

RC - Radio Control

PH - Potential of Hydrogen

DAA- Single Donor, Double Acceptor

DDAA – Double Donor, Double Acceptor

DA - Single Donor and Acceptor

DDA – Double Donor, Single Acceptor

www.manaraa.com

CHAPTER I

INTRODUCTION AND MOTIVATION

1.1 Spectroscopic Methods: Background

Study of absorption and emission of electromagnetic waves by matter and the dependence of these processes on wavelength of these radiations broadly describes the word spectroscopy. The first spectroscope was invented in 1859 by the German chemist, Robert Wilhelm Bunsen and the German physicist, Gustav Robert Kirchhoff to investigate materials which emit light when heated. Since then it has been preeminent in the development of the most fundamental theories in physics, including quantum mechanics, the special and general theories of relativity, and quantum field [1]. When matter interacts with electromagnetic radiation, the sample can either absorb or emit radiation, which in turn is used as an exploratory tool, yielding information about a huge number of different materials. There are wide applications of different spectroscopic techniques depending on the material under investigation such as Raman spectroscopy, (nuclear magnetic resonance) NMR, fluorescence spectroscopy, X-ray spectroscopy etc. [2]. Some spectroscopic techniques access the average or typical properties of a material, while others are employed inside a microscope and can give local information. An example of this would be, a scanning electron microscope that can be used to understand the surface properties of semiconductors and other structures or a scanning tunneling microscope spectroscopic techniques that give insights into electronic structure [2, 3]. Vibrational spectroscopy gives access to information about the molecular structure of the material in its native state. Monitoring changes during degradation,

www.manaraa.com

mechanical load, temperature changes, etc. are possibly due to its non-destructive application *in-situ* studies of performance. Raman scattering occurs as a result of virtual electronic-vibrational transitions and fluorescence occurs due to real electronic transitions. More generally, one can say that fluorescence is an absorption or re-emission process and Raman scattering is an inelastic scattering process.

1.2 Raman Spectroscopy and Plant Science

To meet the needs of the 8.3 billion people projected in 2050, there is a dire need for controlled and efficient crop production using the latest technology [5]. Any type of good crop production calls for intensive research in the area of seeds, soil irrigation, plant growth rate and conditions *in-vivo* and phenotype, studies as well as good storage. Besides a great tolerance of stress conditions like drought, salinity, extreme UV radiation, fungi infections also need to be investigated. In addition, there are environmental impacts of agricultural expansion; viz 2.4 to 2.7-fold increase in nitrogen and phosphorous driven Eutrophication of terrestrial fresh water and near shore ecosystems and vast increase in the pesticides use [6]. Extensive work has already been done to address the above-mentioned factors [5 – 8]. In the present work, an attempt has been made to investigate noninvasive (Raman and fluorescence) spectroscopic methods to predict early stress and improve growth of vegetation. Reflectance spectroscopic methods like chlorophyll fluorescence spectroscopy [10], IR thermal imaging [11], hyperspectral imaging[12], terahertz spectroscopy [13] have all been studies so far. Raman spectroscopy which is a newer technique is a major part of the present thesis. Since Raman technique can observe multiple molecular species simultaneously, three carotenoid peaks were studied under various stress conditions (drought, saline and light). During an abiotic stress, reactive oxygen species (ROS) get collected and plants remove them by producing volatile derivatives and antioxidants [14] and carotenoids peaks show a

www.manaraa.com

decrease at the expense of that. These changes and their trends have been mentioned in the subsequent section 2.3.

1.3 Raman Spectroscopy and Biology

Besides being a tool for physicists, Raman spectroscopy has also become an essential tool for chemists, biologists and materials scientists as well. Complex biological systems like tissues, cells and blood are made up of biomolecules such as proteins, nucleic acids, lipids and carbohydrates. These biomolecules have a unique fingerprint, which enables us to view changes occurring during processes like their thermal denaturation. A class of organic compounds that are fatty acids or their derivatives (cholesterol, cholesterol esters) fall in the category of lipids whose functions include storing energy, signaling, and acting as structural components of cell membranes. Proteins are high molecular weight polypeptides consisting of amino acids and are part of all human body fluids. Changes in the blood protein or lipid amount, as well as the certain fractional quantities, enables for drawing inferences about the human body condition and pathology presence. It sometimes also helps to define the treatment requirements [15]. A mouse is used for modeling human disease because it provides a fine resource of genetic diversity and the capability for extensive gene operation and manipulation [16]. Mice and humans have similar basic bodily operations such as blood cell production (hematopoiesis), digestion, respiration and the cardiovascular system. They are about 3,000 times smaller in size but often respond similarly to humans when they are sick or undergo treatment, which also explains why they are chosen as models. A combination of Raman spectroscopy with multivariate statistical procedures, known as a label-free species-specific diagnostic tool, holds great potential in bio-physics research [16, 17]. The laboratory recombinant inbred (RI) mice with a defined genetic background in which each line can be replicated offers a

www.manaraa.com

number of twins for reproducible data collections. In particular, BXD RI strains produced from parental C57BL/6J and DBA/2J mice [19] demonstrate remarkable differences in red blood cells' (RBCs) membrane rigidity [20]. Therefore, the aim of the study in section 2.4 is to identify the age and gender-specific biomarkers in blood components of the BXD mice using a Raman microscopy set up.

1.4 Raman Spectroscopy and Water

Due to the role that water plays on Earth and in human life, understanding its structure, behavior and properties has been the subject of a number of intensive experimental and theoretical investigations [21] for many years. But until today, there hasn't been complete clearance about changes in its properties that might depend on the environment, the main parameters of which are temperature and pressure. The most informative and non-disturbing method to investigate various media is the Raman scattering of light in them [21, 22]. "Water clusters" are groups of water molecules held together by hydrogen bonds and when seen closely have polar nature, meaning that there is an uneven distribution of electron density. Water has a partial negative charge near the oxygen atom due to the unshared pairs of electrons, and partial positive charges near the hydrogen atoms [24]. Near IR spectrometry has water absorption limitation, whereas Raman technique is relatively insensitive to water, hence is used as a tool to investigate water molecules subject to different polarization of incident light.

A half-wave plate is very handy in rotating the plane of polarization of a polarized source to any other required plane. Most commercial lasers are vertically polarized (perpendicular to the Earth's surface), so to obtain horizontal polarization, one can place a half-wave plate in the beam path with its fast (or slow) axis 45° to the vertical. P and S polarized light on the other hand are defined as light polarized parallel and perpendicular to the plane of incidence

www.manaraa.com

respectively. Using similar source and waveplate, the Raman spectra from deionized water under different polarizations of light source have been investigated in section 2.5 of this thesis and interesting results have been shown.

1.5 Fluorescence Spectroscopy and Portable Systems

Fluorescence has been used as a powerful tool for many decades to explore and evaluate many properties not available to direct observation. Its uses range from medical diagnostics [25], historical monument preservation efforts [26], and water characteristics including potability or identification of organic matter [25, 26] etc. Even though most specimens can be brought into a laboratory for conducting experiments, building mobile laboratories is an intriguing and growing field [28]. A portable spectrophotometer has been designed and tested in Chapter three of this thesis. Portable laser-induced fluorescence systems can cost thousands of dollars and are quite frequently only designed for measurements of certain types of fluorescence [27]. Usually these include photomultiplier tubes (PMT) and filters as their selectors, limiting their use outside of the intended target. The goal of this system was to create a versatile, modular and cost-effective fluorescence system that avoids the shortcomings of these systems and could be integrated into other devices.

1.6 Fluorescence Spectroscopy and Organic Compounds

A LIF sensor has the capability to detect stress in plants and ripeness of fruits mainly by measuring/ monitoring its chlorophyll fluorescence intensity [28, 29]. Hence, application of fluorescence spectroscopy can also be extended for the detection of compounds affecting crops such as the *Aspergillus flavus* fungi and various similar fungal toxins [31]. Detection of these stresses or fungi at an appropriate time can lead to an increase in the crop yield by a considerable

www.manaraa.com

amount. *Polycyclic aromatic hydrocarbons* (PAHs) are usually defined as a group of chemicals with two or more fused benzenoid rings that fluoresce in the visible range. Incomplete combustion of these compounds releases hazardous byproducts in the atmosphere. PAHs are natural constituents of crude oil; therefore, one major way these compounds enter the environment is through automobile emissions. Detection of PAH level content before purchasing gasoline can help to bring down the PAH level in the environment greatly.

1.7 Application to Unmanned Aerial Vehicles

In the last two decades, precision agriculture has been a scientific discipline filed technology that uses new agricultural machinery or air borne platforms equipped with onboard sensors deployed in combination with information systems [7]. Many developments in plant phenotyping are boosted by increasingly available technologies in the field of imaging sensors (like spectrophotometers), and advanced software (for 2D & 3D) image extraction by noninvasive methods. The modularity of the system allowed a base sensor module to connect with an unmanned aerial vehicle (UAV) that flew autonomously in order to perform field surveys. After the flight was completed, the fluorescence spectral data from marked targets and loaded data GPS, time data on ground station was used create a map. Although there are a number of optimizations required for the whole unit to collect data autonomously, this thesis describes the preliminary results for the same.

www.manaraa.com

CHAPTER II

RAMAN SPECTROSCOPY

2.1 Background

Since every compound in nature has a unique fingerprint due to its constituents and their existing states, its identification can be carried out using various methods. Raman spectroscopy provides information about vibrational, rotational, and other low-frequency modes of molecules in a system that can further be used to identify and quantify compounds. The underlying principle (Raman scattering) was discovered in 1928 by V. C. Raman, who won the Nobel prize for his work. Raman spectroscopy is being used in many fields where non-destructive, microscopic, chemical analysis and imaging is required. Another reason Raman spectroscopy has been proposed for interplanetary exploration is that this method of analysis can detect a wide range of inorganic and organic compounds.

2.2 Raman Effect

When light is scattered from a molecule or a crystal, most photons are elastically scattered. The scattered photons have the same energy and wavelength, as the incident photons. However, a small fraction of light (nearly one in ten million photons) is scattered at optical frequencies, hence energies different from the incident photons. This inelastic scattering process is termed as the Raman effect. Raman scattering can occur with a change in vibrational, rotational or electronic energy of a molecule. If the scattering is elastic, the process is called Rayleigh scattering and if it's

www.manaraa.com

not elastic, depending on the energy (frequency) of the emitted photon, the process is called Stokes or anti-Stokes Raman scattering as shown in the Fig. 2.1. The Raman effect arises when a photon is incident on a molecule and interacts with the electric dipole of the molecule.

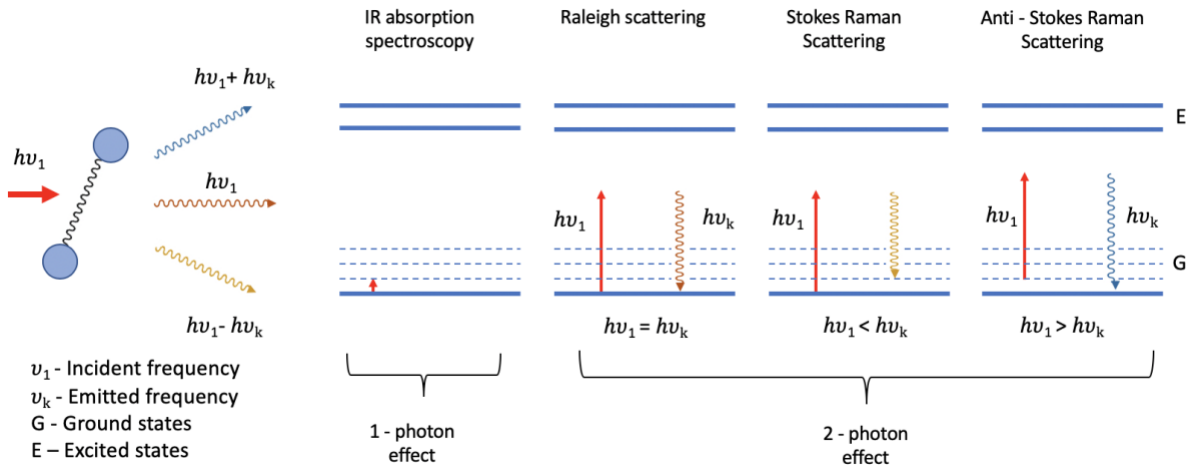

Figure 2.1 Diagrammatic representation of an energy transfer model of IR absorption, Rayleigh scattering, Stokes and anti-Stokes Raman scattering

Absolute wavenumbers: Raman shift (ν) is measured in cm^{-1}

$$\nu\ [cm^{-1}] = \frac{10^7}{\lambda\ [in\ nm\ ]} \tag{2.1}$$

Example: A wavelength of 500 nm corresponds to 2000 cm^{-1} (wavenumber)

Relative wavenumber:

$$\nu\ [cm^{-1}] = \frac{10^7}{\lambda_{exc}\ [in\ nm\ ]} - \frac{10^7}{\lambda_{sc}\ [in\ nm\ ]} \tag{2.2}$$

Example: A Raman band at 1020 cm^{-1} and excited with a laser wavelength of 500 nm scatters light at a wavelength 527 nm.

www.manaraa.com

2.3 Stress in Vegetation

2.3.1 Background

In anticipation of rising population (and in turn higher food demand), the ability to measure stress in vegetation using *in-vivo* techniques is rapidly becoming vital for increasing agricultural production and research. Even a subtle change in surrounding environment and composition of the vegetation land such as drought, temperature, light, salinity, and PH during the growing season of plant strongly affect the plant metabolism. It is estimated that these factors are responsible for more than 50 % crop yield losses in major plants. Abiotic stresses like drought, salinity, light exposure and chilling temperature are considered to be the major environmental constraints that the plant has to cope with. Recently, it has been demonstrated in the previous collaborative research work that Raman spectroscopy plays an important role to detect abiotic stress responses [31, 32]. Raman spectroscopic technique is used here to detect a fingerprint of chemical bonds by which molecules can be identified. Carotenoids [34] can be categorized as compounds, mostly hydrocarbon chains with alternating double and single bonds between the carbon atoms that absorb in the visible part of the spectrum. Length of the polyene chain in the compounds is inversely proportional to the energy of absorption and the lower bond order between the carbon atoms sinks the vibrational energy of the carbon–carbon double bond. A pure ethylenic bond frequency is approximately around 1650 cm^{-1}, but the Raman frequency of polyenes is lower than 1600 cm^{-1}, with longer chain polyenes producing lower frequency Raman bands [34, 35].

The changes of Raman spectral intensities in controlled and stressed plants are monitored in a controlled environment to assess stress-induced responses in the plant, as a good complement to, or better than, the other existing techniques (i.e., fluorescence method), towards high-throughput stress phenotyping in plants.

www.manaraa.com

2.3.2 Experimental Set-up and Calibration

The experimental layout of confocal Raman set-up is as shown in Fig. 2.2. A tunable continuous wave laser (wavelength: 532 nm, beam diameter: 3 mm) purchased from Civil Lasers with an adjustable power supply was used as an excitation source, which was collimated using two 1-inch silver coated mirror (Thorlabs). The collimated beam was incident on a dichroic mirror (cut-off long pass filter: 550 nm, Thor lab), which was focused onto the sample using 1-inch converging lens (focal length: 10 cm, Thorlabs). The sample i.e. leaves of plants were placed at the focus of lens. Raman signal and reflected laser from the sample then passed through the lens and dichroic mirror. After passing through dichroic mirror, two one-inch (focal length: 2.54 cm) convex lenses help to collimate the reflected Raman signal from the sample. A notch filter (Thorlabs) was introduced in the path of signal which collected the Raman signal (Stokes) and filtered out the Raleigh and anti-Stokes light reaching the detector. To align the signal on the slit of spectrometer two 1-inch silver coated mirrors were used and a two-inch converging lens (focal length: 10 cm) was mounted in 1D manual stage that focused the signal into opening slit of the spectrometer (*Andor*) with EMCCD (electron multiplied charged couple device), deeply cooled digital camera (air-cooled up to -60 ºC). In order to prevent the spectrometer from saturation, a neutral density filter wheel (Thorlabs) with varying filtrations was placed in between the lens and slit of the spectrometer.

www.manaraa.com

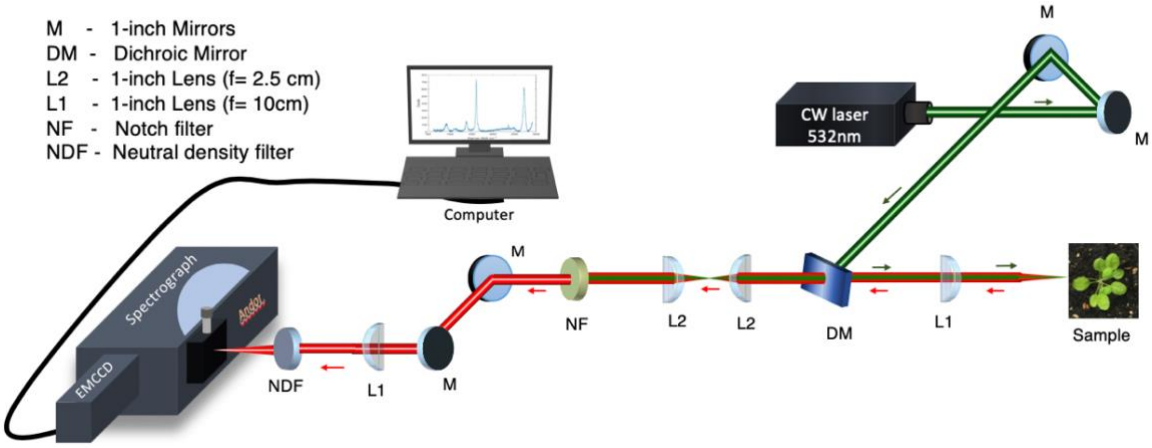

Figure 2.2 Raman spectroscopic layout (excitation laser: 532 nm)

Calibration of the spectrometer was done by comparing characteristic peaks of the spectra obtained from helium and hydrogen bulbs (Mississippi State University) and the Raman spectra of the two available in literature [37]. The system was calibrated using equation for a linear fit:

$$\nu 1\ [cm^{-1}] = I_0 + C_1 * \nu 2\ [cm^{-1}] \quad (2.3)$$

ν_1 = Calibrated wavenumber

ν_2 = Uncalibrated wavenumber

I_0 = Fit constant

C_1 = Fit coefficient

www.manaraa.com

Calibration using helium lamp is demonstrated as follow:

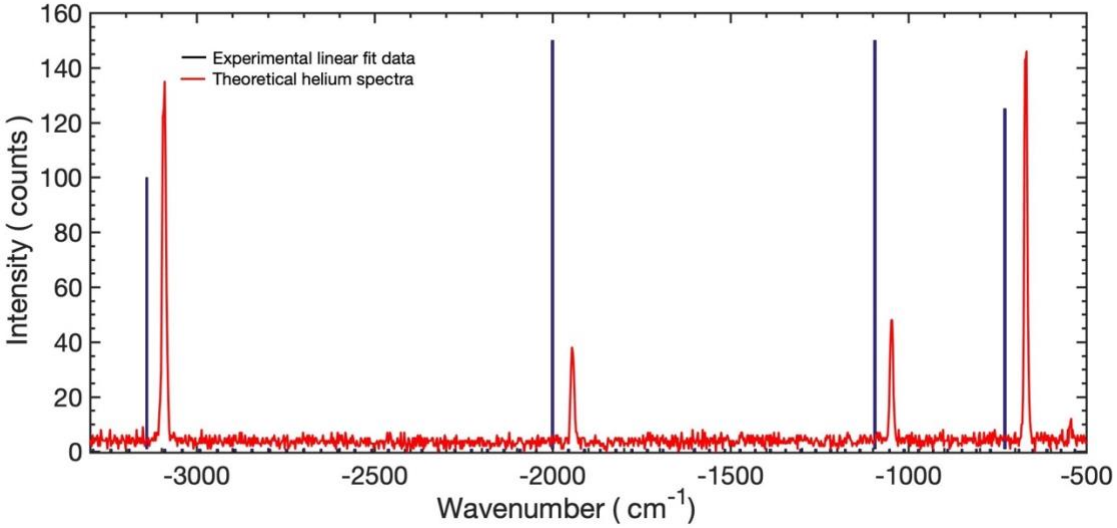

Figure 2.3 Uncalibrated helium spectra (red) along with theoretical helium characteristic peaks (black)

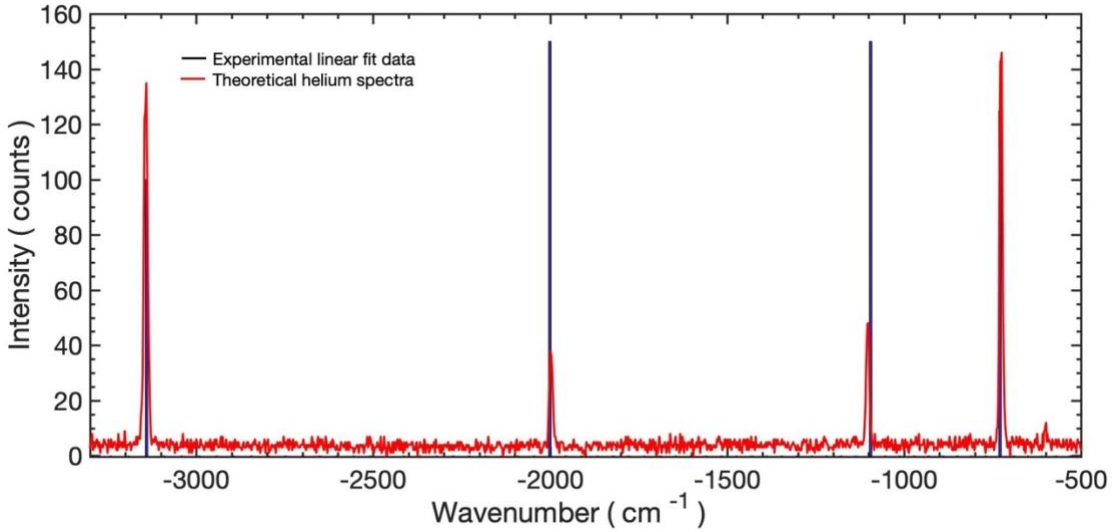

Figure 2.4 Calibrated helium spectra (red) along with theoretical helium characteristic peaks (black)

www.manaraa.com

2.3.3 Drought and Saline Stress

2.3.3.1 Sample Preparation and Data Acquisition

Arabidopsis Thaliana plants (four weeks in age) were procured from the department of plant physiology (Mississippi State University). After giving the plants two days to adjust to the new surrounding with 16 hours of light/8 hours of dark cycle using LED grow lights (photosynthetic photon flux density, PPFD ~ 600 μmol /m^2 /s) and normal watering (once a day), they were separated into different trays: controlled plants, drought stress plants, saline stress plants and light stress (discussed in section 2.3.4) plants. To mirror the effect of salt and drought stress, the plants were watered with 200 mM solution of NaCl solution instead of usual water. Normal watering was withheld to create the drought stress. Plant responses with above two stress were recorded over the course of one week in every 12 hours duration using the Raman spectroscopy system. The same part of the leaf was used to take data every time by placing it directly in the focal point of the excitation laser without physical detachment from the plant. Therefore, it is considered as *in-vivo* measurement. The slit of the spectrometer was opened manually to collect the Raman signal. Raman spectra were recorded from the samples using the spectrometer with the help of *Solis* software that comes with the spectrometer. The set-up was optimized using pyridine sample every time before taking any sets of data. A grating (that bends the Raman shifted light according to wavelength) of 1200 lines/mm was used. All Raman peaks were observed in the wavelength range 550 - 610.93 nm with the laser power of 1.2 μW and acquisition time was ten seconds. Five sets of data were taken sequentially for each plant.

www.manaraa.com

2.3.3.2 Analysis

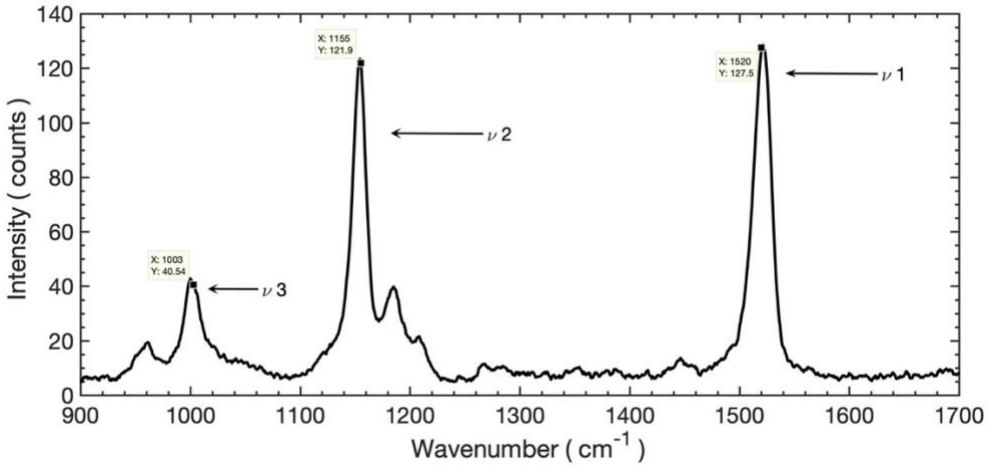

Figure 2.5 Averaged and baseline corrected Raman spectra of control *Thaliana* leaf with an integration time of ten seconds and groove setting as 1200 lines/mm
Main characteristic peaks of carotenoids (ν_1,ν_2 and ν_3) used in this study are marked with their corresponding wavenumbers

The intrinsic fluorescence background can sometimes be orders of magnitude stronger than the Raman scattering (in the case of a dying plant), so background removal has been one of the foremost challenges for quantitative analysis of Raman spectra in many samples [38].

Data was saved in ascii file format by *Solis* software. Saved data files were imported in university provided *MATLAB* and processed further by taking the mean of the spectra for each sample and correcting the baseline by fitting it with polynomial of order seven and multiple iterations. A model of the processed data is shown in Fig. 2.5 with main carotenoid peaks labeled.

The data was fairly spread out, ergo a linear regression model was used to fit the data for all three peaks separately to see and compare the differences in the trend line for all of the plots.

www.manaraa.com

2.3.3.3 Results

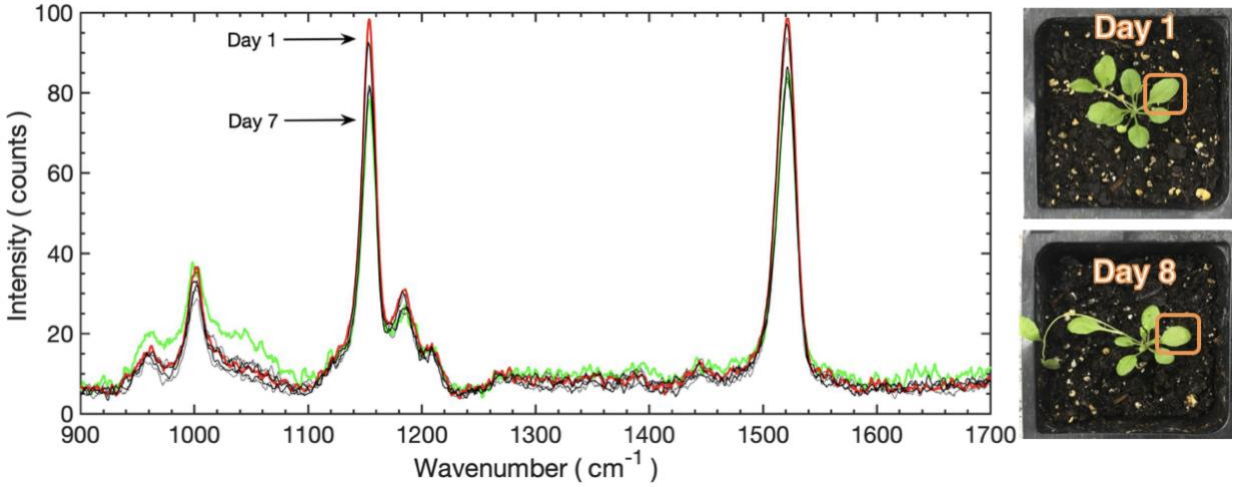

Figure 2.6 (left) Averaged and baseline corrected Raman spectra of control *Thaliana* leaf taken over the course of seven days
(right) Picture of the plant used with marked leaf portion to acquire data on day one and day eight: corresponding spectra are marked with colors red and green respectively

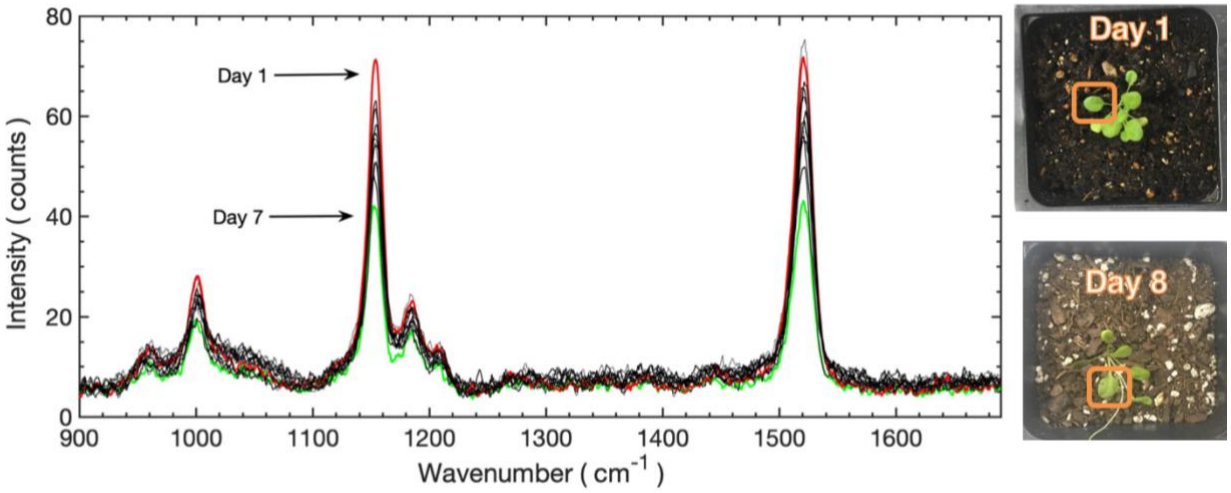

Figure 2.7 (left) Averaged and baseline corrected Raman spectra of drought *Thaliana* leaf taken over the course of seven days
(right) Picture of the plant with marked leaf portion to acquire data on day one and day eight: corresponding spectra are marked with colors red and green respectively

www.manaraa.com

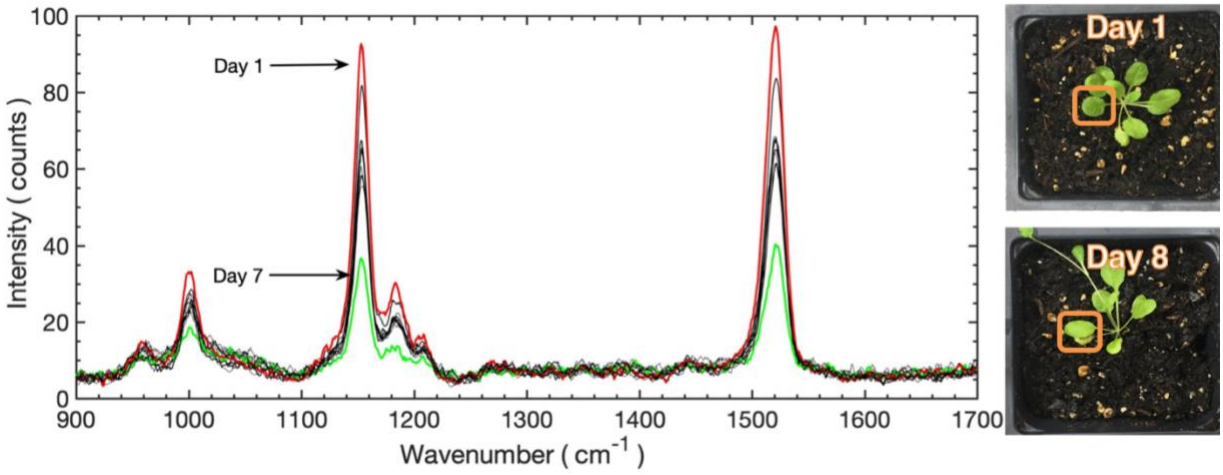

Figure 2.8 (left) Averaged and baseline corrected Raman spectra of saline *Thaliana* leaf taken over the course of seven days
(right) Picture of the plant with marked leaf portion to acquire data on day one and day eight: corresponding spectra are marked with colors red and green respectively

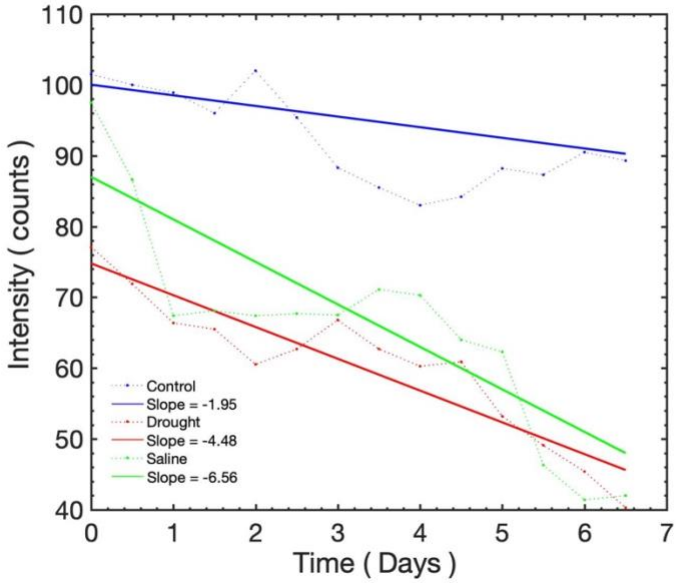

Figure 2.9 Peak intensity of ν_1 (C=C stretching vibrations) vs Days for control (blue), drought (red) and saline (green) linearly regressed with corresponding lines depicting the trend in changes over the course of seven days

www.manaraa.com

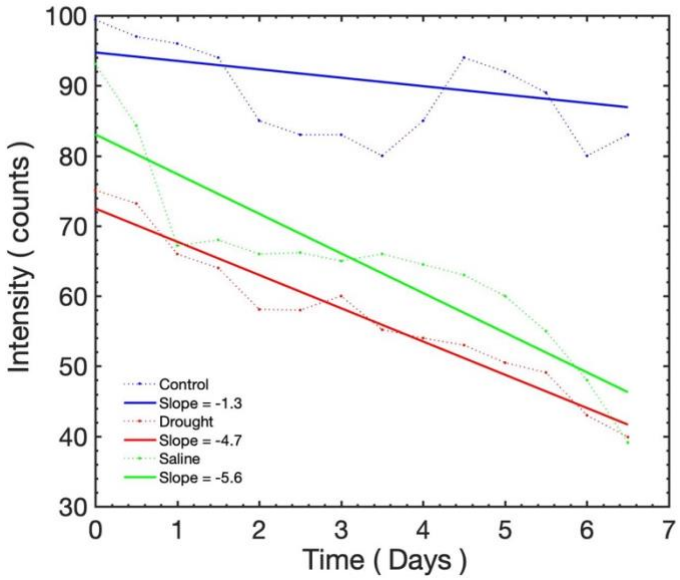

Figure 2.10 Peak intensity of ν_2 (C-C stretches coupled either to C-H in-plane bending or C-CH_3 stretching) vs Days for control (blue), drought (red) and saline (green) linearly regressed with corresponding lines depicting the trend in changes over the course of seven days

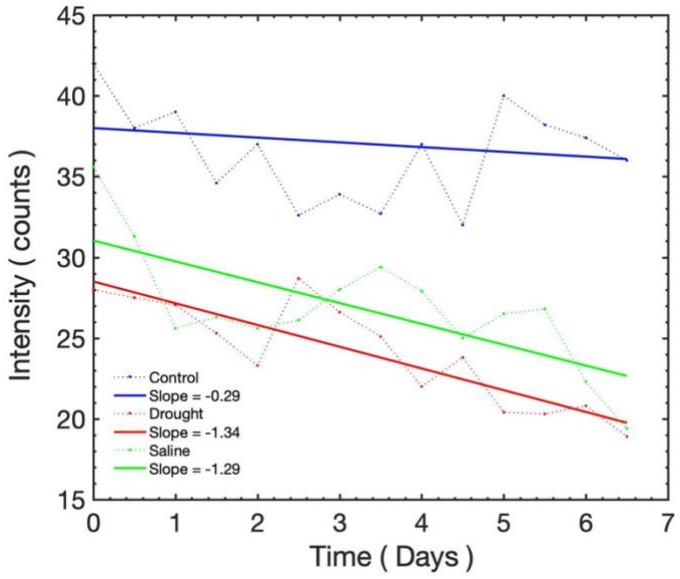

Figure 2.11 Peak intensity of ν_3 (CH_3 in-plane rocking vibrations) vs Days for control (blue), drought (red) and saline (green) linearly regressed with corresponding lines depicting the trend in changes of the peak over the course of seven days

www.manaraa.com

Figures 2.6, 2.7 and 2.8 show the changes in the spectra over the course of seven days for control, drought and saline respectively (red being the spectra for first day and green for seventh day). Although the control was not as consistent as expected ideally, it is evident in the graph of saline and drought plants that the stress considerably reduces all the peaks way more than the peaks in control plants over the days. Since the data points acquired were scattered, a linear fit (y= mx + b) was used to find the trend lines for the data points. Fig. 2.9, 2.10 and 2.11 are plotted to show the relative difference in the trend lines of the three carotenoid peaks ν_1, ν_2 and ν_3 with respect to days, in drought and saline conditioning and a controlled environment.

Peak ν_1 is attributed to the C=C stretching vibrations [39], decreased by 13%, 40.2% and 57.7% for control, drought and saline plants respectively. The trend lines shown for ν_1 for all three plants shown in Fig. 2.9 also depicts the same. The slope of control was -1.95, whereas the slope of lines that linearly fit the data for drought and saline were -4.48 and -6.56 respectively. Peak ν_2 assigned to C-C stretches coupled either to C-H in-plane bending or C-CH_3 stretching, decreased by 19%, 42.2% and 59.3% in control, drought and saline plants over the time period and the trend lines had a slope of -1.3, -4.7 and -5.6 for the same as shown in Fig. 2.10. Peak ν_3 assigned to C-CH_3 in-plane rocking vibrations overall decreased by 0.02%, 32% and 42% for control, drought and saline whose trend lines had a slope of -0.29, -1.34, -1.29 respectively as shown in Fig. 2.11. Saline and drought have a noticeably higher slope of dropping as compared to control for all three peaks. To make sure the results were unbiased, the spectra was taken using the same predetermined spot (marked in Fig. 1.4,1.5 and 1.6) on the leaves for all plants. Comparing the pictures of day one and day seven, the changes in the plant peaks were observed before a naked eye could see a visible change in the plant, thereby making this methodology robust for future study in early detection of plant stress.

www.manaraa.com

2.3.4 Light Stress

2.3.4.1 Sample Preparation and Data Acquisition

For light stress the plants were continuously exposed to the LED grow lights (PPFD ~ 600 µmol /m^2 /s) without any dark period and data was taken until 24 hours of exposure of light (beyond the usual 16 hours of light) at different intervals of time (1, 2, 4, 8, 10, 12 and 24 hours). The parameters for data acquisition were kept same as mentioned in section 2.3.3.1. The same part of the leaf was used to take data every time by placing it directly in the focal point of the excitation laser without physical detachment from the plant.

2.3.4.2 Analysis

Data was saved in ascii file format by *Solis* software. Saved data files were imported in university provided *MATLAB* and processed further by taking the mean of the spectra for each sample and correcting the baseline by fitting it with polynomial of order seven. A model of the processed data is shown in Fig. 2.5 with main carotenoid peaks labeled. The intensity of all three carotenoid peaks considered were noted at each time interval and were plotted individually against hours of stress delivered to the plant. The results of the graphs yielded by the peaks of the two plants are shown in the next section.

www.manaraa.com

2.3.4.3 Results

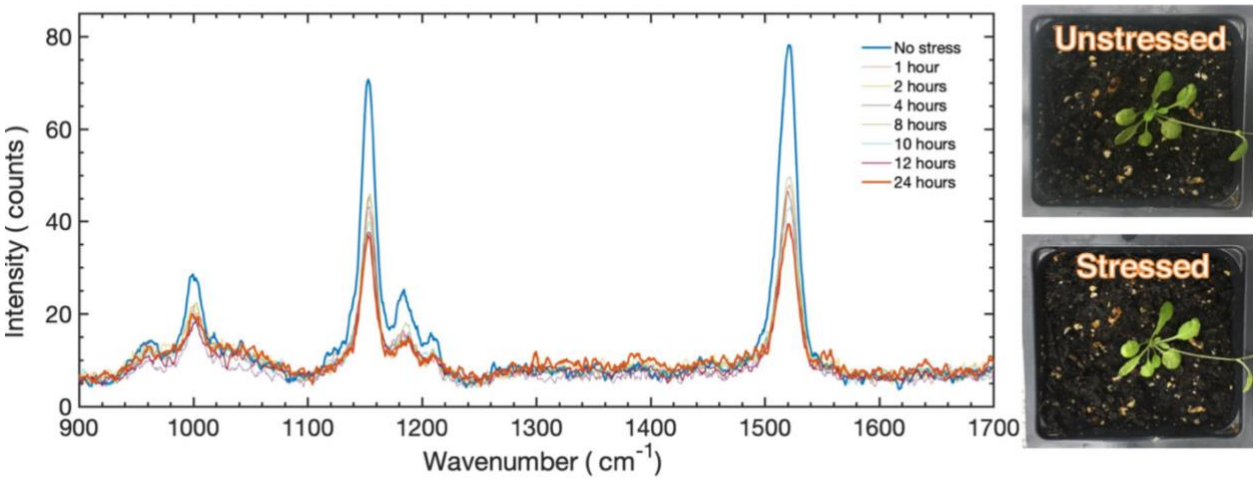

Figure 2.12 (left) Averaged and baseline corrected Raman spectra of *Thaliana* (plant 1) leaf taken over the course of several hours (marked in top right)
(right) Picture of the plant used with marked leaf portion to acquire data with no stress and stressed for 24 hours: corresponding spectra colors are blue and red respectively

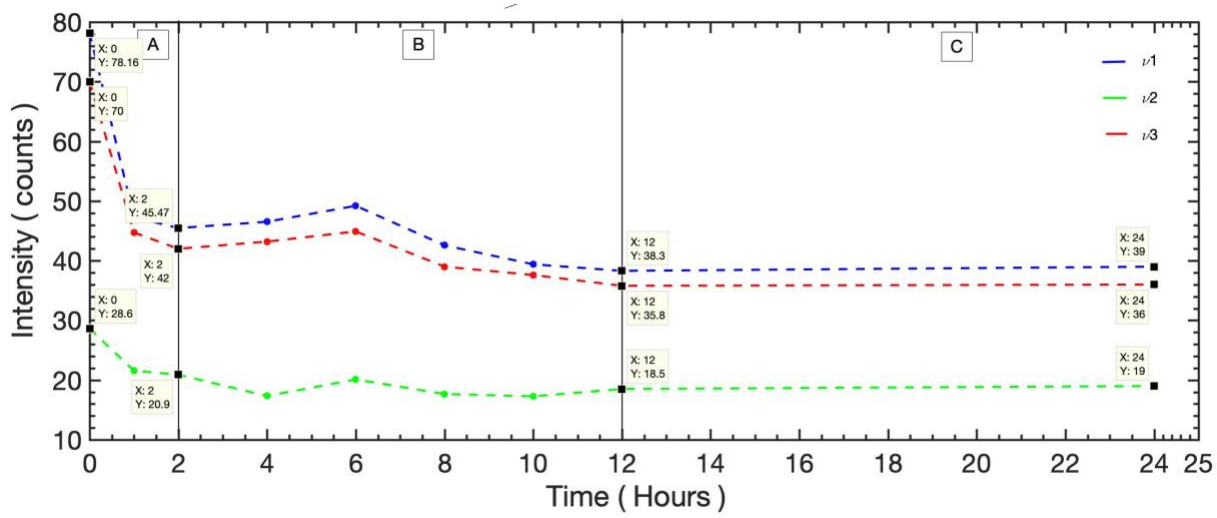

Figure 2.13 Peak intensities vs hours for ν_1 (blue), ν_2 (red) and ν_3 (green)
Three regions attributed to stress, recover/coping and acclimation to light stress are marked as A, B and C respectively

www.manaraa.com

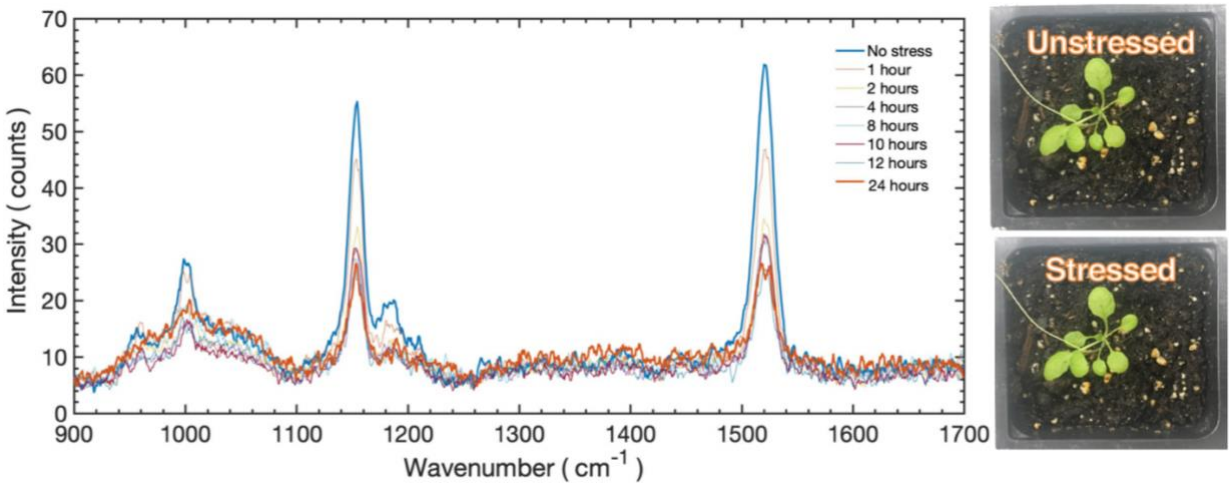

Figure 2.14 (left) Averaged and baseline corrected Raman spectra of *Thaliana* (plant 2) leaf taken over the course of several hours (marked in top right)
(right) Picture of the plant used with marked leaf portion to acquire data with no stress and stressed for 24 hours: corresponding spectra colors are blue and red respectively

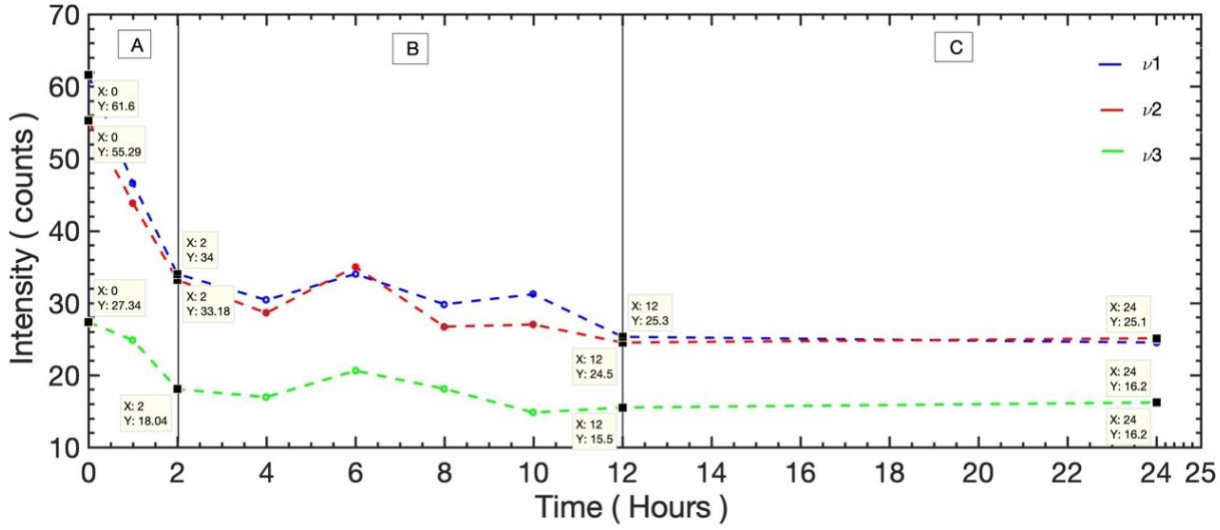

Figure 2.15 Peak intensities vs hours for ν_1 (blue), ν_2 (red) and ν_3 (green)
Three regions attributed to stress, recover/coping and acclimation to light stress are marked as A, B and C respectively

www.manaraa.com

Figures 2.12 and 2.14 show the spectral characteristics of the two plants at various time intervals, with and without affected by light stress. Figures 2.13 and 2.15 show the variations in the three carotenoid peaks ν_1, ν_2 and ν_3, with respect to the hours of exposure time for two different plants. (zero hour is attributed to the time when the plants were not stressed with light at all). The peak values in both the graphs show a similar trend, they decreased by about 40% in the first two hours and fluctuated in the next eight hours, past which they became nearly constant.

The three regions A, B and C, in the carotenoid peak intensity vs hours graph can be visualized as major stress, recovery or coping and acclimatization regions, respectively. The constant part in both graphs can be explained by the fact that plants have a mechanism to acclimate to stress, that might have been activated after a certain point in time (about 12 hours), especially *Arabidopsis Thaliana* [39 – 41]. The plants were fairly young in age; hence, it can be hypothesized that these plants acclimate to the excess light [43].

2.3.5 Future Scope

Therefore, Raman spectroscopy gives high throughput stress phenotyping and early stress detection, however a major drawback of Raman spectroscopy is its impoverished repeatability, which makes it hard to obtain reliable quantitative measurements [44]. Even though the quantities might not be same when repeated, the trends in the peak changes with stress should remain similar to the above-mentioned results hence should be able to be further investigated.

www.manaraa.com

2.4 Murine Blood Components

2.4.1 Background

Blood makes up to seven to eight percent of the total body weight and performs innumerable, inevitable functions required for healthy living. Plasma is the liquid component of the blood in which red blood cells (erythrocytes) and white blood cells (leukocytes) are suspended. It constitutes more than half of the blood's volume and consists mostly of water that contains dissolved salts (electrolytes) and proteins. Serum, however, is the left-over supernatant fluid after coagulated blood has been centrifuged and comprises of hormones, glucose, electrolytes, antigens, Albumin, Globulin, nutrients and proteins. Since Serological testing can diagnose multiple illnesses it is of great importance in the field of biomedical research. The presence of certain types of antibodies can also mean that a person is immune to one or more antigen. This means that future exposure to the antigen won't result in illness. Albumin is a versatile carrier protein which is synthesized in the liver and acts as the transporter of fatty acids, hormones and other compounds. It makes up to 60% protein present in the blood and is a negative acute phase reactant, the blood component levels of which decrease by approximately 30% in response to disease, tissue injury or inflammation. Its secondary structure, containing 67% helical structures next to 10% turn, and 23% extended chain configurations without any β sheets, strongly affect its properties. The most distinct and characteristic Raman bands of these are the amide signatures around 1600 cm^{-1} [45], 1160 cm^{-1} (deformation vibrations of CC group), 1250 cm^{-1} (α-helix in Amide III), 1330 cm^{-1} (vibrations of tryptophan), 1450 cm^{-1} (deformation vibrations of -CH_2 group), 1650 cm^{-1} (β-helix in Amide I) [50] and lipids around 2952 cm^{-1} [46]. Since it can provide a chemical fingerprint of structures and molecular conformation within the sample, combining a Raman spectrometer to a

www.manaraa.com

standard optical microscope set-up allows high magnification visualization of a sample and Raman analysis with a microscopic laser spot that in turn has many advantages for biological research.

2.4.2 Experimental Set-up

Experimental set-up used is schematically presented in Fig. 2.16. A thermally stabilized continuous-wave laser (as used previously) was employed to produce the beam for excitation of the sample molecules. The probing laser was reflected by a dichroic mirror and focused by the objective lens (magnification:10 X and numerical aperture:0.40) onto the sample. The scattered radiation was collected and directed into the spectrometer via the notch filter, which helps in eliminating the laser radiation from the recorded signal. Raman signal was collected and imaged on the entrance slit of the spectrograph with EMCCD (*Andor*).

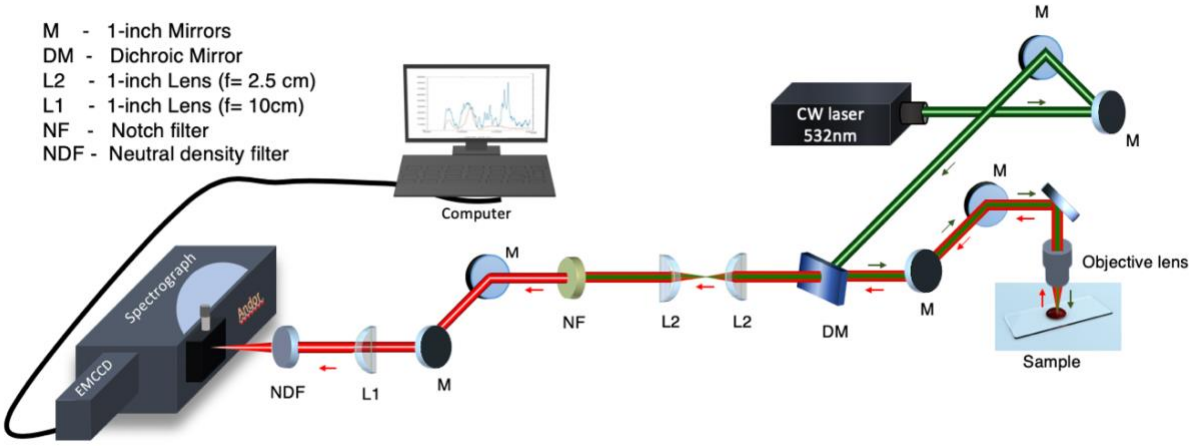

Figure 2.16 Raman micro spectroscopic set-up with objective lens magnification:10 X, numerical aperture: 0.40

www.manaraa.com

2.4.3 Sample Preparation and Data Acquisition

Mice blood samples were transported from the University of Tennessee Health Science Center (UTHSC) lab and stored at -80 C for a week. The samples consisted of seven C57BL/6J (strain) and eight DBA/2J (strain) mice blood samples with varying gender and ages in between four to ten months. On the day of the experiment the samples were allowed to thaw for an hour before the collection of data started. Once the samples were thawed, a drop (~ 0.1 ml) of each sample was cautiously poured over a glass slab and placed under the microscope to be analyzed at fast speeds. A manual XYZ stage was used to optimize the signal obtained by adjusting the focus of the objective lens onto the sample. The diameter of the laser probing beam was 3 mm and effective laser power 12 mW whereat laser irradiation volume scattered into the glass slide with the sample. Such level of power per unit area excludes the possibility of thermal damage of blood proteins in the sample. Raman spectroscopic analysis was performed with an acquisition time of one second and 32 spectra were taken from three locations for each specimen (two with blood and one without blood i.e., empty glass). The experiment was performed at room temperature. Since refreezing albumin is not a favorable process (since it disrupts the chemical profile) all data collection was done on the same day. All spectra were recorded in 563-638 nm spectral range with integration time of 1 second and the total time of spectra registration was 32 seconds per sample. Groove setting was set to 600 lines/mm for wider field of view.

www.manaraa.com

2.4.4 Analysis

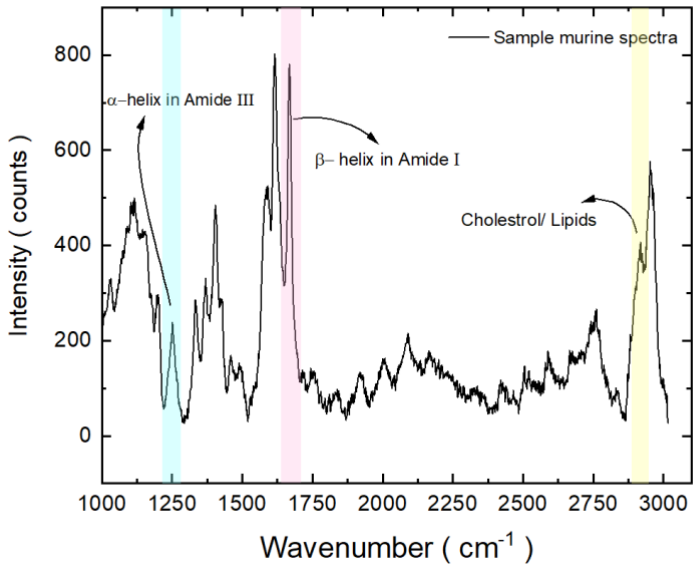

Figure 2.17 Averaged and baseline corrected Raman spectrum of mice blood
Peak assigned to some amide bands and lipids have been highlighted [45, 46]

2.4.4.1 Principal Components Analysis

Principal component analysis (PCA) is a multivariate ordination analysis used as a tool to reduce multidimensional data to lower dimensions while retaining most of the information. It pretends to order samples in a plane defined by the number of principal components (Example: PC1 and PC2 will define a 2D plane according to their continuous variable values). PCA helps to measure the total variability among the samples. The total variability will always be 100%, however even though the PCs reach up to 99% to explain the variability in the data, it can never be 100, but is enough for result interpretation. Because the PCA is a transformation of the old coordinate system (peaks) into the new coordinate system (PC), it can be estimated how much each of the old coordinates (peaks) contribute to each of the new ones (PCs). These values are

www.manaraa.com

called loadings. The higher the loading of a particular peak onto a PC, the more it contributes to that PC. An eigenvalue and its corresponding eigenvector in the newly formed PCs space explain how much variance there is in the data in that direction. The eigenvector with the highest eigenvalue is therefore the principal component that explains maximum information. The covariance value indicates the correlation between two variables, and the matrices of covariance show the inter-correlations among all parameters [48].

2.4.4.2 Data Processing

The raw data was pre-processed (mean of 30 data sets of blood sample and polynomial fit to order nine for each sample) in *MATLAB.* In order to reduce the background due to fluorescence or other disturbances, the data was further imported into *OriginLab* and PCA was performed on the data using the "*PCA for spectroscopy"* application in the software. The age of the samples was included as an additional factor. After a few trials, the number of components to be extracted was set to three. The scree plot, loading with reference spectrum plot, score plot and eigenvalues table were obtained and further used for interpretation of the results.

2.4.5 Results

Table 2.1 Covariance matrix table showing eigenvalues and percentage of variance for principal components

Principal Component Number	Eigenvalues	Percentage of Variance (%)	Cumulative (%)
1	0.00000014	73.04	73.04
2	3066330.56	16.17	89.20
3	1004808.54	5.30	96.58
4	393825.28	1.43	98.02

www.manaraa.com

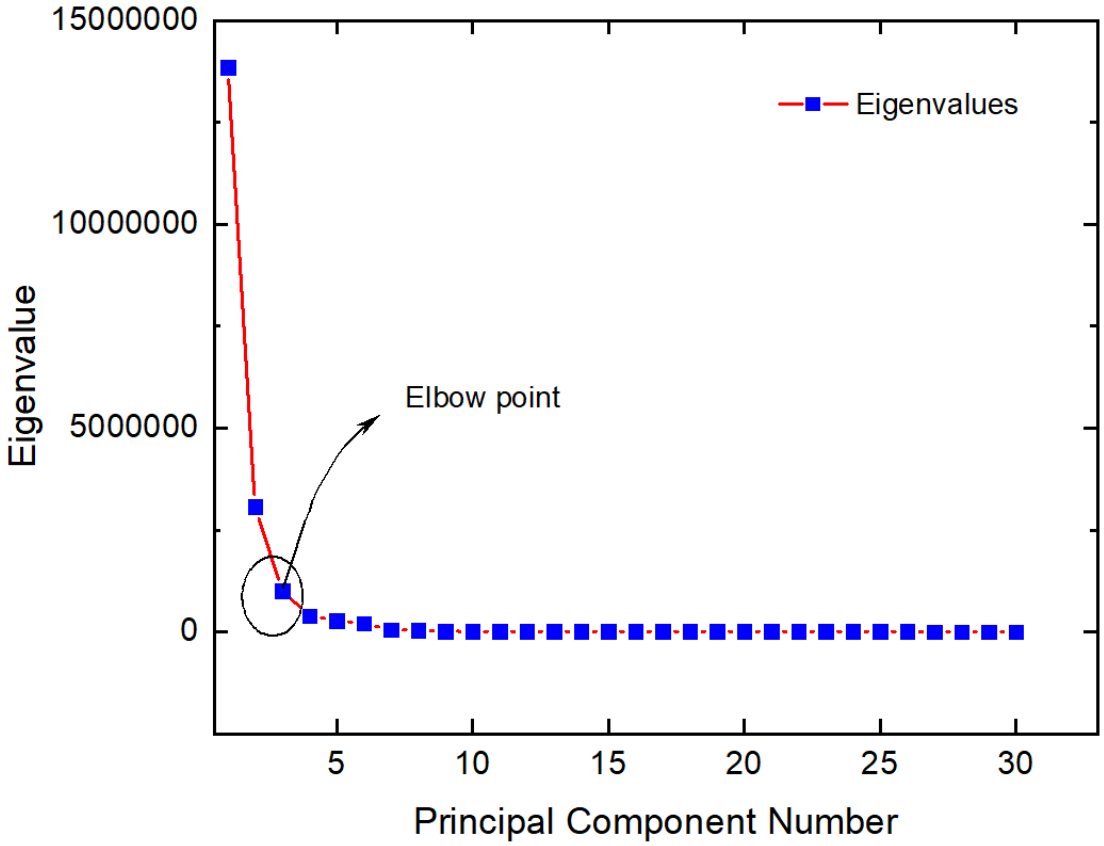

Figure 2.18 Scree Plot: The 'elbow' point in this plot confirms three principal components that can be used to explain maximum variance in the data

www.manaraa.com

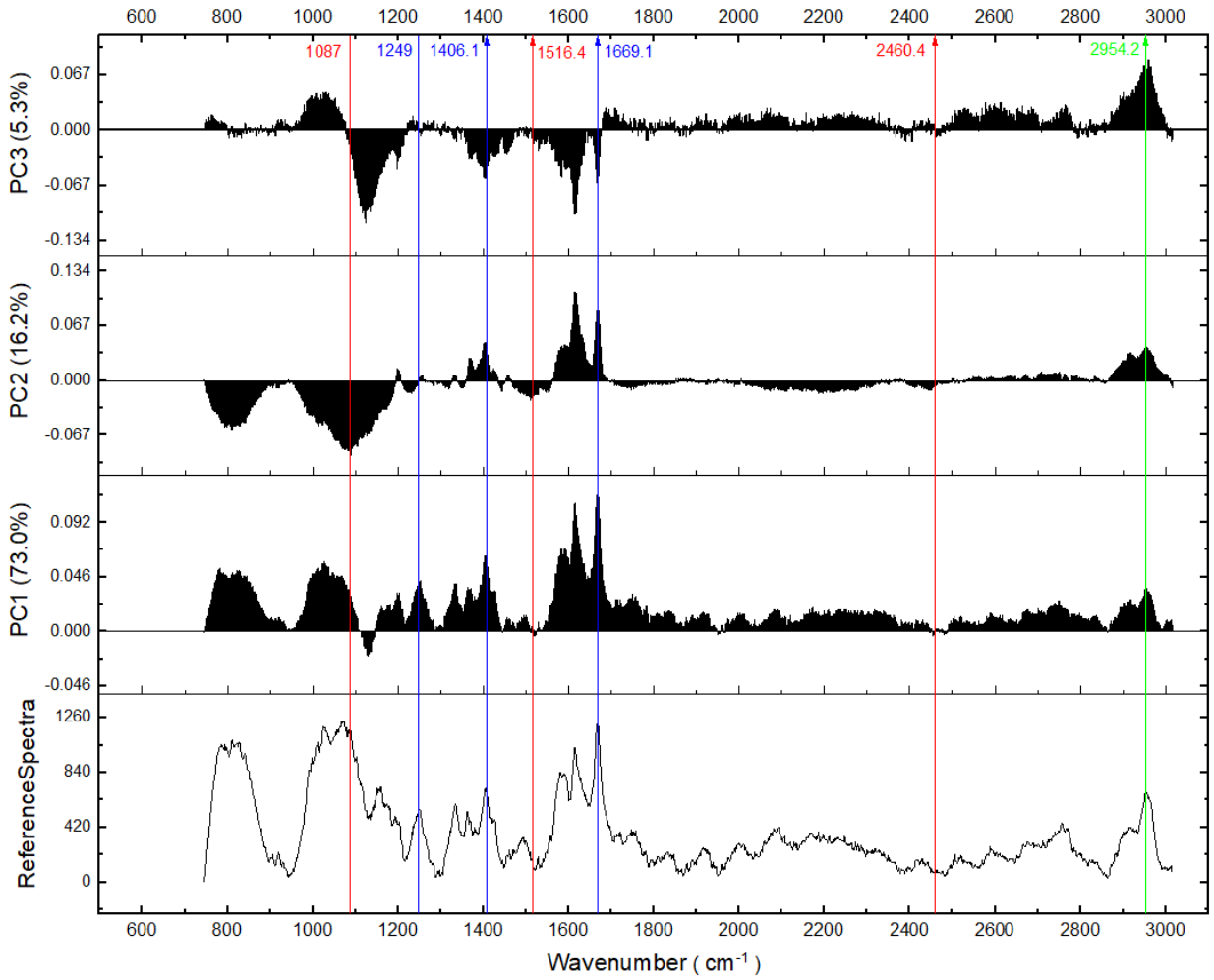

Figure 2.19 Loading with Reference Spectrum Plot: This plot shows an estimate of how much each of the old coordinates (example: marked peaks) contribute to each of the new coordinates, namely PC1, PC2 and PC3

www.manaraa.com

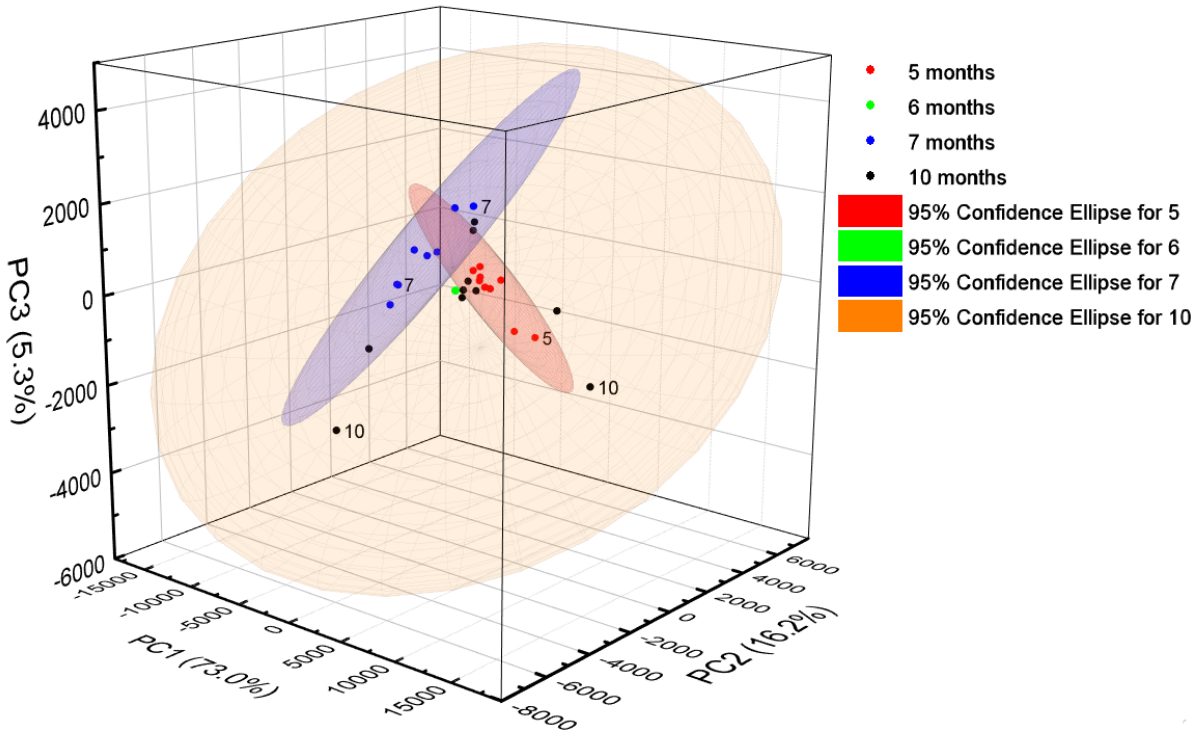

Figure 2.20 Score Plot: Depicting segregation of samples in the new PC space on the basis of age

In the eigenvalues of the Covariance Matrix table (Table 2.1), we can see that the first three principal components explain over 96% of the variance and the remaining components each contribute 5% or less. Therefore, three main components are kept. A scree plot shown in Fig. 2.18 was used as a visual aid for determining the appropriate number of principal components as well. The number of components chosen are equal on the 'elbow' point after which the remaining eigenvalues are relatively small and not as significant. This point is evident in the scree plot and confirms number of main components to be extracted as Figure 2.18 shows, so we can say the third point is our 'elbow' point. In Fig. 2.19, the first layer shows the spectrum of the reference sample, the second layer illustrates loading for the first component, the third layer for the second

www.manaraa.com

component and the fourth layer for the third component. The graph shows that wavenumbers, 1249, 1406 and 1669 cm^{-1} are more significant in PC1, while wavenumbers 1087, 1516 and 2460 have more weight in PC2 and wavenumber 2954 is most significant in PC3. These peaks can be assigned to lipids (band near 2950 cm^{-1}) [46], possible contribution from albumin (protein bands around 600 to 1300 cm^{-1} also known as Amide III bands) and the Amide I band (around 1669 cm^{-1}) [47, 49]. The Fig. 2.20 illustrates scores of 15 samples of mice blood components (two data set for reach sample, so the total is 30) in PC1, PC2 and PC3 space. The samples were of varying ages. It is clear from the graph that five-month-old and seven-month-old mice can be divided easily in principal component space, while ten-month-old samples intersect with the five-month samples. The ellipses shown in the figure are the confidence ellipses of scores for the three groups of samples respectively and outliers are marked.

2.4.6 Future Scope

In further work, PCA can be incorporated with the partial least squares method to solve quantitative problems or explain the outliers and/or overlapping regions in the component space.

www.manaraa.com

2.5 Water Subject to Polarized Light

2.5.1 Background

Despite its prevalence and importance, water in the form of liquid is not as well understood as in its other phases. With a change in physical state the structure of water also changes, however, in all states, water is a polar molecule with electron-deficient hydrogen atoms and an electron-rich oxygen atom. This polarity difference enables hydrogen bonding interaction between water molecules. The water molecule is composed of hydrogen and oxygen, in a ratio of two volumes of hydrogen for one volume of oxygen. Raman spectra in the range of 1600 cm^{-1} and 4000 cm^{-1} in liquid water are well explained by molecular vibration modes of a temporal C_{2v} tetrahedral-like structure around oxygen atom [50].

Raman spectroscopy occurs as a result of a molecular vibration causing a "change in polarizability" of the molecule, therefore being an appropriate tool to investigate tectonic behavior of water. In the high frequency region, the Raman spectrum of water is comprised of five sub-bands, which are located at 3014, 3226, 3432, 3572, and 3636 cm^{-1}, and can be assigned to *v*DAA-OH, *v*DDAA-OH, *v*DA-OH, *v*DDA-OH, and free OH symmetric stretching vibrations, respectively (D- donor, A- acceptor, OH- Oxygen Hydrogen) [51].

Spectra of water and its structure also have a dependence on temperature, however, at most temperatures the two most intensive constituent peaks are observed around 3230 and 3440 cm^{-1} line in the OH stretch region, and their total contribution to the Raman spectrum of water is higher than 90% [52]. Out of these two peaks, one peak stretches symmetrically and the other one has an asymmetric stretch with respect to principal axis of symmetry [53]. In addition to the general method, application of polarized Raman rules (E.g. Porto's notation: can be helpful in assigning vibrational modes, particularly symmetry of vibrational modes, identification and differentiation

www.manaraa.com

of allotropes and different crystal forms of elements and compounds and also helps in characterizing and detecting disorders and directionally varying strain.

2.5.2 Experimental Set-up

The set-up is shown in Fig. 2.19. The laser used here had a default vertical linear polarization (100:1). The apparatus used is similar to the Raman set-up as in section 2.3.2, with an additional introduction of a 1-inch half-wave retarder in the path of the collimated beam from the laser reaching the dichroic mirror. A polarizing cube beam splitter that allows only parallel polarized light to pass through is also set between the lens L1 and the entrance slit of the spectrometer.

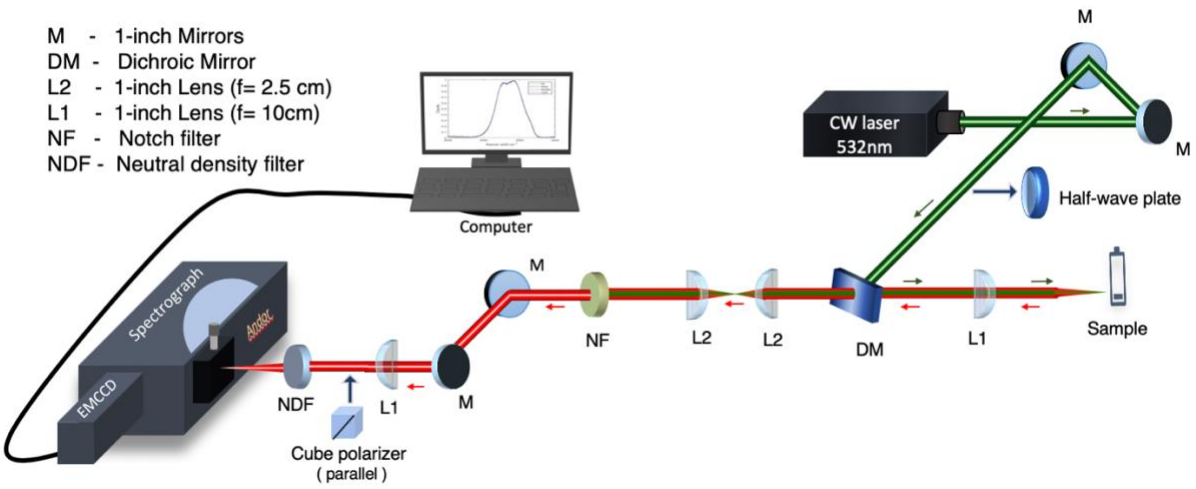

Figure 2.21 Polarized Raman spectroscopic set-up

www.manaraa.com

2.5.3 Sample Preparation and Data Acquisition

Deionized water was procured from the Geoscience Department (Mississippi State University) and using a pipette was carefully put in a 2 mm glass cuvette. The cuvette was sealed and put vertically at the focus of the lens (L1 before sample). The half-wave retarder used was set at five different angles (equal intervals in between 0^o to 90^o : changing polarization from P to S at 45^o and back to P at 90^o). RS analysis was performed in order to record three spectral data (range 2500 to 4000 cm^{-1}) from one location on the cuvette for each angle setting with acquisition time of ten seconds and laser power 7 mW. The groove setting was 1200 lines/mm for good resolution of the spectral features. Temperature and humidity during the experiment were set to 72 F and 40% RH respectively.

www.manaraa.com

2.5.4 Analysis

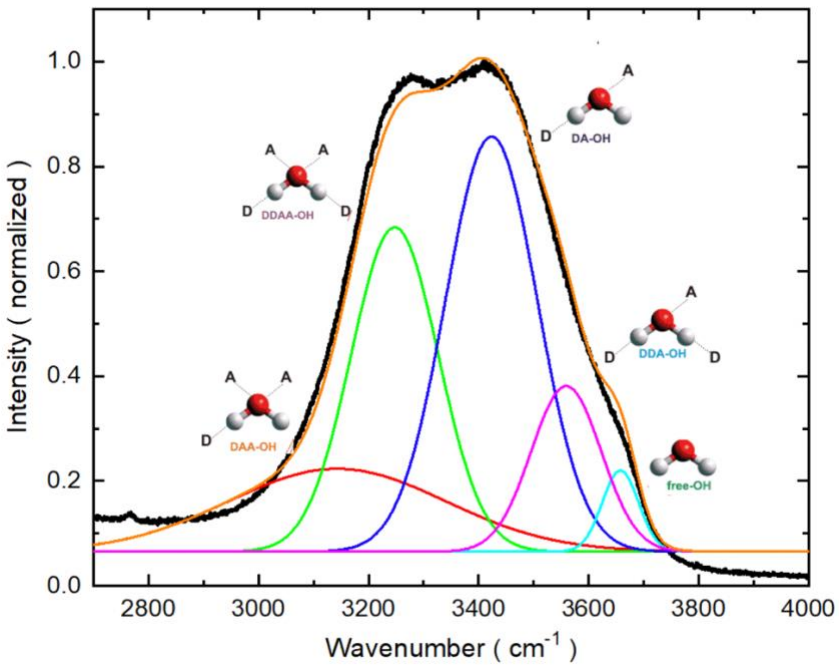

Figure 2.22 Raman spectrum of DI water is shown in black. This spectrum is deconvoluted into five constituents with positions of peaks near 3074, 3225, 3432, 3575 and 3640 cm^{-1}

2.5.4.1 Deconvolution using Gaussian Fits

Spectroscopic, chromatographic and other forms of data sometimes contain multiple, often overlapping peaks. Deconvolution is a process where a mathematical function (in the current experiment a, Gaussian peak) is used to fit determined experimental data and to separately determine contribution of each peak to the spectrum. Usually it helps us observe features that are hidden by stronger signals, or to see shifts that the raw experimental data do no show clearly, among other observations.

www.manaraa.com

The R^2 value, which is also known as the coefficient of determination (COD), is a statistical measure to qualify peak fitting. It is a percentage of the response variable variation that is explained by the fitted curve. For example, the resulted R^2 value of a fit explains approximately more than that much percentage of the variability in the response variable. Hence, R^2 is always between zero and one. The closer the fit is to the data points, the closer R^2 will be to the value of 1 [54].

After the data was downloaded from the software, it was exported in *OriginLab*. Raw data was first normalized and then a peak fitting analysis was performed using Gaussian curves. The peaks were fit to converge using multiple iterations and the value of peak area, FWHM, wavenumber was noted.

Gaussian equation used in *OriginLab*:

$$y(x) = y_0 + \frac{A*exp(-4*ln(2)*(x-x_c)^2/\ w^2\ )}{(w*sqrt[\pi/(4*ln(2))])} \tag{2.4}$$

Where,

y_0 – base intensity

w - FWHM

A – Area

x_c – Center wavenumber

www.manaraa.com

2.5.5 Results

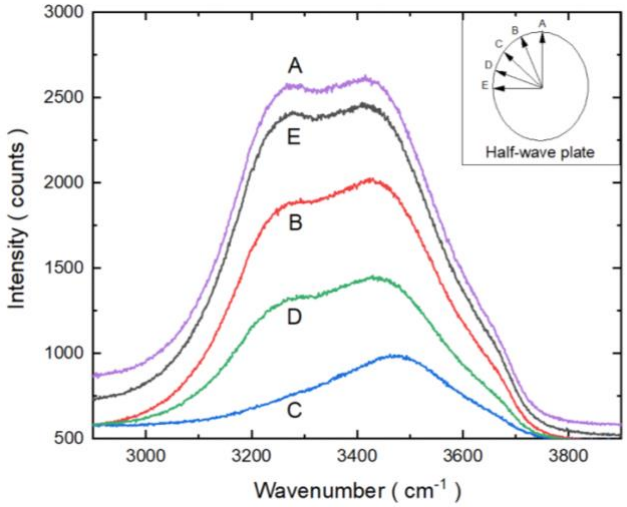

Figure 2.23 Unprocessed Raman spectrum of DI water at different positions of half-wave retarder as marked; changing polarization from P (position A) to S (position C) at 45º and back to P at 90º (position E) along with spectra at two more intermediate angles (position B and D of the retarder)

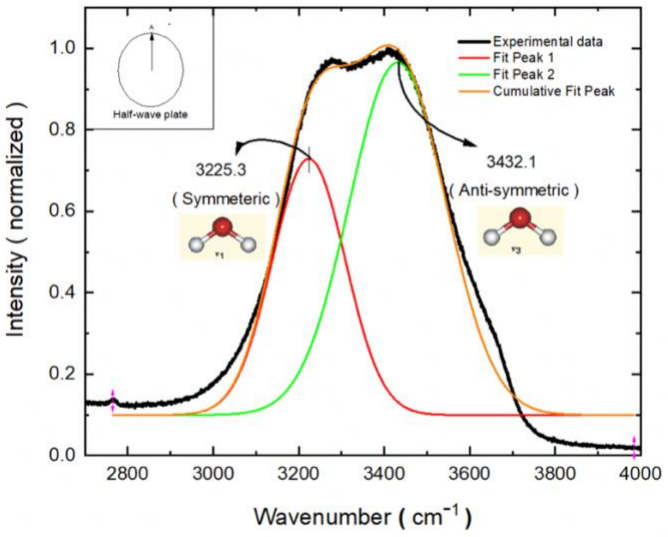

Figure 2.24 Normalized Raman spectrum of DI water (black), with half-wave retarder at position A. The spectra are deconvoluted into two main component peaks around 3225 and 3432 cm^{-1}

www.manaraa.com

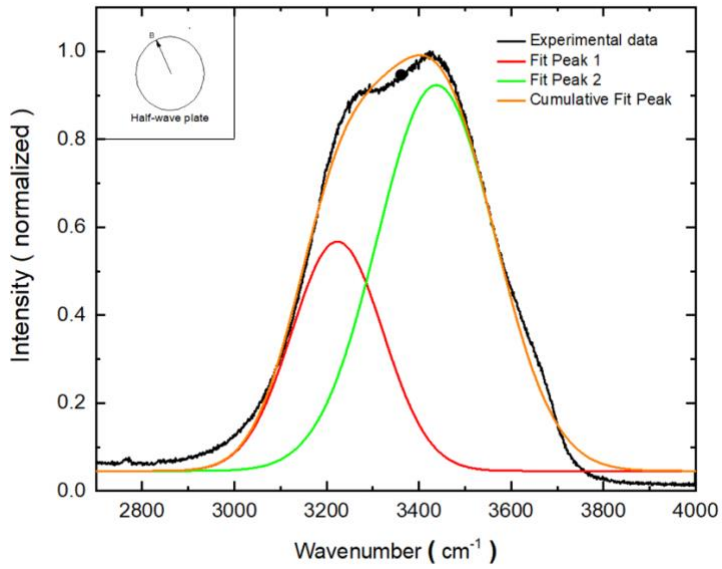

Figure 2.25 Normalized Raman spectrum of DI water (black) with half-wave retarder at position B. Peak around 3225 cm^{-1} of deconvoluted spectra showing a slight decrease, and the deconvoluted peak around 3432 cm^{-1} remained same

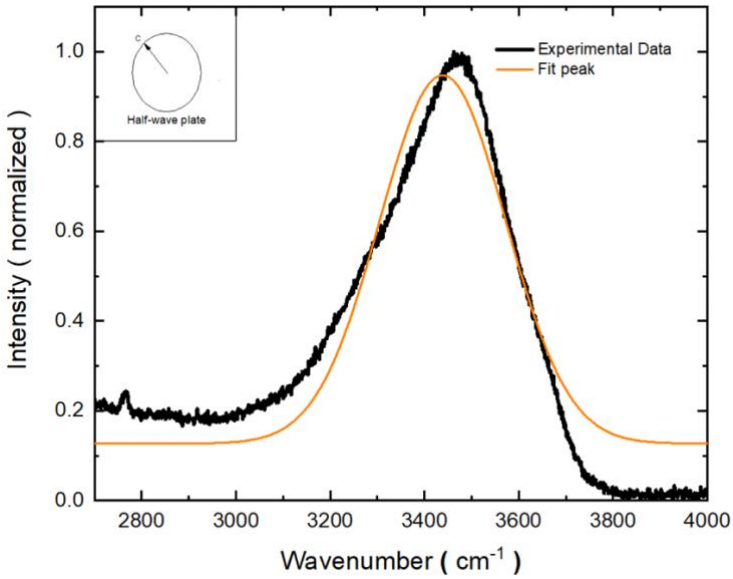

Figure 2.26 Normalized Raman spectrum of DI water (black) with half-wave retarder at position C depicting the disappearance of the symmetric stretching peak

www.manaraa.com

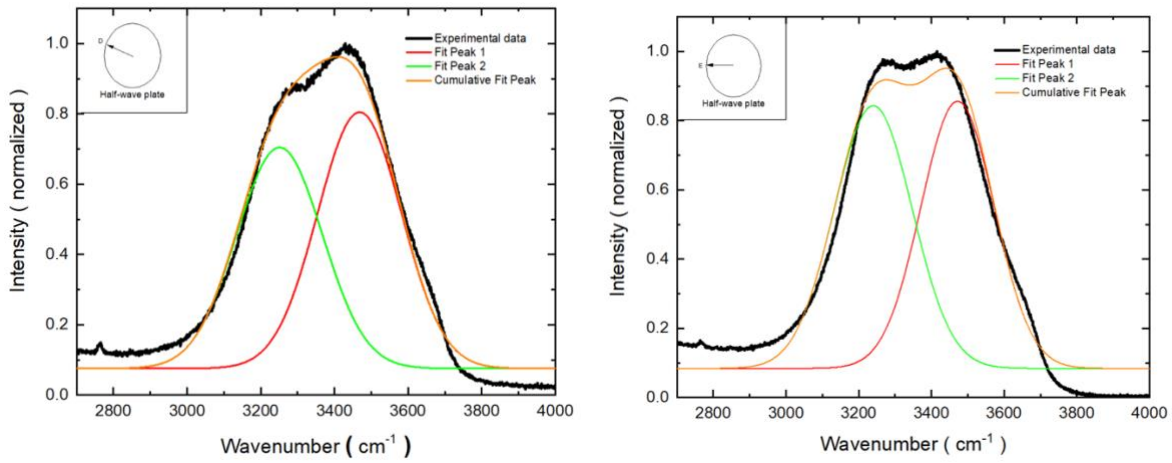

Figure 2.27 (left) Normalized Raman spectrum of DI water (black) with half-wave retarder at position D with similar results of Fig. 2.23 for deconvoluted peak positions. (right) Normalized Raman spectrum of deionized water (black) with half-wave retarder at position E with similar results at Fig. 2.24 for deconvoluted peak positions

2.5.6 Discussion and Future Scope

Figure 2.23 shows the raw spectrums obtained at five different positions of the half waveplate (A through E). A half-wave retarder introduces a phase of Π radians between perpendicular axes. Rotating it by theta (Θ) relative to the polarization direction shifts polarization angle by 2Θ, hence when plate is rotated by 45^o (position C) the polarization changes from P to S. Figure 2.24 shows the normalized spectra of water (black) and two Gaussian fitted peak models with wavenumbers 3225.3 (symmetric stretch) and 3432.1(antisymmetric stretch) at position 'A' of the half-wave plate. FWHM for these peaks were 171 and 225 and areas of peak were 135 and 244 respectively. The coefficient of determination (or goodness of fit was 0.98).

Figure 2.25 shows the normalized spectra of water (black) and two gaussian fitted peaks with wavenumbers 3225.3 and 3432.1 at position 'B' of the half-wave plate. FWHM for these peaks were 171 and 225 and areas were 129 and 280 respectively. The coefficient of determination for

www.manaraa.com

the fit was 0.99. Figure 2.26 shows the normalized spectra of water (black) and one gaussian fitted peak with wavenumber 3455 at position 'C' of the half-wave plate. FWHM and area for the fitted peak were 314 and 275 respectively. The coefficient of determination for the fit was 0.99. There was a slight shift noted in the wavenumber of the assigned peak.

Figure. 2.27 (left) shows the normalized spectra of water (black) and two gaussian fitted peaks with wavenumbers 3223.6 and 3438.1at position 'D' of the half-wave plate. FWHM for these peaks were 271 and 268 and areas were 183 and 208 respectively. The coefficient of determination for the fit was 0.98. Figure. 2.27 (right) shows the normalized spectra of water (black) and two gaussian fitted peaks with wavenumbers 3226.1 and 3434.1 at position 'E' of the half-wave plate. FWHM for these peaks were 253 and 237 and areas were 203 and 195 respectively. The coefficient of determination for the fit was 0.97.

In the high-frequency region (OH stretch region), as shown in the parallel and perpendicular polarized configurations, both of the normal vibrational modes can be assigned based on their energies and polarization responses. One system of bands in the liquid phase is associated with symmetric (low-frequency) OH vibration of water molecule with is polarized and another system of vibrational bands is associated with the "antisymmetric" (high-frequency) vibration which is depolarized. Therefore, as the angles were increased from 0º to 90º as shown in the Figure. 1.22, the peak at (3432 cm^{-1}) started to disappear and at 45º (cross polarized) the only peak visible in the spectrum was around (3455 cm^{-1}), confirming it is depolarized. Reproducing the results obtained and investigate frequency shift in the second peak at S polarization using approaches that have been used previously by other groups can be a potential project for further investigation [54, 55].

www.manaraa.com

2.6 References

[1] D. W. Ball, "Spectroscopy is applied quantum mechanics, Part III: Introduction to quantu...: Universitat Autònoma de Barcelona," *Spectroscopy*, 2008.

[2] K. F. Lim and S. W. Lewis, "Spectroscopic Techniques," in *Encyclopedia of Forensic Sciences: Second Edition*, 2012.

[3] O. L. Krivanek *et al.*, "Vibrational spectroscopy in the electron microscope," *Nature*, 2014.

[4] B. C. Stipe, M. A. Rezaei, and W. Ho, "Single-molecule vibrational spectroscopy and microscopy," *Science (80-.).*, 1998.

[5] N. E. Borlaug, "Ending World Hunger. The Promise of Biotechnology and the Threat of Antiscience Zealotry," *Plant Physiol.*, vol. 124, no. 2, pp. 487–490, Jul. 2002.

[6] D. Tilman *et al.*, "Forecasting agriculturally driven global environmental change," *Science (80-.).*, vol. 292, no. 5515, pp. 281–284, Apr. 2001.

[7] F. Fiorani and U. Schurr, "Future Scenarios for Plant Phenotyping," *Annu. Rev. Plant Biol.*, vol. 64, no. 1, pp. 267–291, Mar. 2013.

[8] M. A. K. Jansen, V. Gaba, and B. M. Greenberg, "Higher plants and UV-B radiation: Balancing damage, repair and acclimation," *Trends in Plant Science*, vol. 3, no. 4. Elsevier Ltd, pp. 131–135, 01-Apr-1998.

[9] L. Bernstein, "Effects of Salinity and Sodicity on Plant Growth," *Annu. Rev. Phytopathol.*, vol. 13, no. 1, pp. 295–312, Jul. 2003.

[10] H. M. Kalaji, K. Bosa, J. Kościelniak, and Z. Hossain, " Chlorophyll a Fluorescence—A Useful Tool for the Early Detection of Temperature Stress in Spring Barley (Hordeum vulgare L.) ," *Omi. A J. Integr. Biol.*, vol. 15, no. 12, pp. 925–934, Nov. 2011.

[11] S. Zia *et al.*, "Infrared Thermal Imaging as a Rapid Tool for Identifying Water-Stress Tolerant Maize Genotypes of Different Phenology," *J. Agron. Crop Sci.*, vol. 199, no. 2, pp. 75–84, Apr. 2013.

[12] J. Behmann, J. Steinrücken, and L. Plümer, "Detection of early plant stress responses in hyperspectral images," *ISPRS J. Photogramm. Remote Sens.*, vol. 93, pp. 98–111, 2014.

[13] N. Born *et al.*, "Monitoring Plant Drought Stress Response Using Terahertz Time-Domain Spectroscopy," *PLANT Physiol.*, vol. 164, no. 4, pp. 1571–1577, Apr. 2014.

[14] K. Apel and H. Hirt, "Reactive oxygen species: metabolism, oxidative stress, and signal transduction.," *Annu. Rev. Plant Biol.*, vol. 55, pp. 373–99, 2004.

المنارة للاستشارات
www.manaraa.com

[15] E. B. Hanlon *et al.*, "Prospects for in vivo Raman spectroscopy," *Physics in Medicine and Biology*, vol. 45, no. 2. Feb-2000.

[16] T. A. Partridge, "The mdx mouse model as a surrogate for Duchenne muscular dystrophy," *FEBS Journal*, vol. 280, no. 17. pp. 4177–4186, Sep-2013.

[17] D. W. Shipp, F. Sinjab, and I. Notingher, "Raman spectroscopy: techniques and applications in the life sciences," *Adv. Opt. Photonics*, vol. 9, no. 2, p. 315, Jun. 2017.

[18] K. J. I. Ember *et al.*, "Raman spectroscopy and regenerative medicine: a review," *npj Regen. Med.*, vol. 2, no. 1, Dec. 2017.

[19] J. L. Peirce, L. Lu, J. Gu, L. M. Silver, and R. W. Williams, "A new set of BXD recombinant inbred lines from advanced intercross populations in mice," *BMC Genet.*, vol. 5, Apr. 2004.

[20] C. A. Schaefer and M. J. Dewey, "Single locus (rol) control of extreme resistance to red cell osmotic lysis: Intrinsic mode of gene action," *Genetics*, vol. 121, no. 2, pp. 353–358, 1989.

[21] D. W. Ball, "Theory of Raman Spectroscopy," 2001.

[22] M. Harvey, "Properties of water," in *Drinking Water: A Socio-Economic Analysis of Historical and Societal Variation*, Taylor and Francis Inc., 2015, pp. 1–20.

[23] C. L. Braun and S. N. Smirnov, "Why is water blue?," *J. Chem. Educ.*, vol. 70, no. 8, p. 612, Aug. 1993.

[24] F. H. Stillinger and C. W. David, "Polarization model for water and its ionic dissociation products," *J. Chem. Phys.*, vol. 69, no. 4, pp. 1473–1484, 1978.

[25] S. Andersson-Engels, C. A. Klinteberg, K. Svanberg, and S. Svanberg, "In vivo fluorescence imaging for tissue diagnostics," *Phys. Med. Biol.*, vol. 42, no. 5, pp. 815–824, May 1997.

[26] S. Svanberg, "Fluorescence Spectroscopy and Imaging of Lidar Targets," 2010, pp. 433–467.

[27] P. Chen, D. Pan, and Z. Mao, "Development of a portable laser-induced fluorescence system used for in situ measurements of dissolved organic matter," *Opt. Laser Technol.*, vol. 64, pp. 213–219, 2014.

[28] H. Morillas, M. Maguregui, J. Trebolazabala, and J. M. Madariaga, "Nature and origin of white efflorescence on bricks, artificial stones, and joint mortars of modern houses evaluated by portable Raman spectroscopy and laboratory analyses," *Spectrochim. Acta - Part A Mol. Biomol. Spectrosc.*, 2015.

www.manaraa.com

[29] I. Urbano Bron, R. Vasconcelos Ribeiro, M. Azzolini, A. Pedro Jacomino, and E. Caruso MacHado, "Chlorophyll fluorescence as a tool to evaluate the ripening of 'Golden' papaya fruit," *Postharvest Biol. Technol.*, vol. 33, no. 2, pp. 163–173, Aug. 2004.

[30] K. Maxwell and G. N. Johnson, "Chlorophyll fluorescence - A practical guide," *Journal of Experimental Botany*, vol. 51, no. 345. Oxford University Press, pp. 659–668, 2000.

[31] M. C. Rodríguez, G. H. Sánchez, M. S. Sobrero, A. V. Schenone, and N. R. Marsili, "Determination of mycotoxins (aflatoxins and ochratoxin A) using fluorescence emission-excitation matrices and multivariate calibration," *Microchem. J.*, vol. 110, pp. 480–484, Sep. 2013.

[32] N. Altangerel *et al.*, "In vivo diagnostics of early abiotic plant stress response via Raman spectroscopy," *Proc. Natl. Acad. Sci.*, vol. 114, no. 13, pp. 3393–3396, Mar. 2017.

[33] C. Surridge, "Remote phenotyping: Raman reveals stress," *Nat. Plants 2017 34*, Apr. 2017.

[34] H. K. Lichtenthaler and J. A. Miehé, "Fluorescence imaging as a diagnostic tool for plant stress," *Trends Plant Sci.*, vol. 2, no. 8, pp. 316–320, Aug. 1997.

[35] A. V. Ruban, A. A. Pascal, B. Robert, and P. Horton, "Configuration and Dynamics of Xanthophylls in Light-harvesting Antennae of Higher Plants," *J. Biol. Chem.*, vol. 276, no. 27, pp. 24862–24870, Jul. 2001.

[36] H. Schulz, M. Baranska, and R. Baranski, "Potential of NIR-FT-Raman spectroscopy in natural carotenoid analysis," *Biopolymers*, vol. 77, no. 4, pp. 212–221, Mar. 2005.

[37] G. H. Watson and W. B. Daniels, "Raman scattering from dense helium and argon," *Phys. B+C*, vol. 139–140, pp. 472–474, May 1986.

[38] P. J. Cadusch, M. M. Hlaing, S. A. Wade, S. L. McArthur, and P. R. Stoddart, "Improved methods for fluorescence background subtraction from Raman spectra," *J. Raman Spectrosc.*, vol. 44, no. 11, pp. 1587–1595, Nov. 2013.

[39] M. Macernis *et al.*, "Resonance Raman spectra of carotenoid molecules: Influence of methyl substitutions," *J. Phys. Chem. A*, vol. 119, no. 1, pp. 56–66, Jan. 2015.

[40] F. K. Choudhury, A. R. Devireddy, R. K. Azad, V. Shulaev, and R. Mittler, "Rapid Accumulation of Glutathione During Light Stress in Arabidopsis," *Plant Cell Physiol.*, vol. 59, no. 9, pp. 1817–1826, Sep. 2018.

[41] P. A. Crisp *et al.*, "Rapid Recovery Gene Downregulation during Excess-Light Stress and Recovery in Arabidopsis," *Plant Cell*, vol. 29, no. 8, pp. 1836–1863, Aug. 2017.

المنارة للاستشارات
www.manaraa.com

[42] P. A. Crisp, D. Ganguly, S. R. Eichten, J. O. Borevitz, and B. J. Pogson, "Reconsidering plant memory: Intersections between stress recovery, RNA turnover, and epigenetics," *Sci. Adv.*, vol. 2, no. 2, p. e1501340, Feb. 2016.-'

[43] F. Ramel *et al.*, "Light-Induced Acclimation of the Arabidopsis chlorina1 Mutant to Singlet Oxygen," *Plant Cell*, vol. 25, no. 4, pp. 1445–1462, Apr. 2013.

[44] D. Dong and C. Zhao, "Limitations and challenges of using Raman spectroscopy to detect the abiotic plant stress response," *Proc. Natl. Acad. Sci.*, vol. 114, no. 28, pp. E5486–E5487, Jul. 2017.

[45] C. G. Atkins, K. Buckley, M. W. Blades, and R. F. B. Turner, "Raman Spectroscopy of Blood and Blood Components," *Applied Spectroscopy*, vol. 71, no. 5. SAGE Publications Inc., pp. 767–793, 01-May-2017.

[46] K. Czamara, K. Majzner, M. Z. Pacia, K. Kochan, A. Kaczor, and M. Baranska, "Raman spectroscopy of lipids: A review," *Journal of Raman Spectroscopy*, vol. 46, no. 1. John Wiley and Sons Ltd, pp. 4–20, 17-Nov-2015.

[47] A. Rygula, K. Majzner, K. M. Marzec, A. Kaczor, M. Pilarczyk, and M. Baranska, "Raman spectroscopy of proteins: A review," *Journal of Raman Spectroscopy*, vol. 44, no. 8. pp. 1061–1076, Aug-2013.

[48] "Principal Component Analysis (PCA) Basics."

[49] N. Kuhar, S. Sil, T. Verma, and S. Umapathy, "Challenges in application of Raman spectroscopy to biology and materials," *RSC Advances*, vol. 8, no. 46. Royal Society of Chemistry, pp. 25888–25908, 2018.

[50] Y. Tominaga, A. Fujiwara, and Y. Amo, "Dynamical structure of water by Raman spectroscopy," *Fluid Phase Equilib.*, 1998.

[51] Q. Sun, "The Raman OH stretching bands of liquid water," *Vib. Spectrosc.*, vol. 51, no. 2, pp. 213–217, Nov. 2009.

[52] S. M. Baschenko and L. S. Marchenko, "On Raman spectra of water, its structure and dependence on temperature," *Semicond. Physics, Quantum Electron. Optoelectron.*, vol. 14, no. 1, pp. 77–79, 2011.

[53] D. Tuschel, "Practical Group Theory and Raman Spectroscopy, Part I: Normal Vibrational Modes," *Spectroscopy*, 2014.

[54] Caltech. University, "Statistics and the Treatment of Experimental Data." [Online]. Available: https://ned.ipac.caltech.edu/level5/Leo/Stats2_3.html. [Accessed: 17-Jun-2019].

www.manaraa.com

[55] B. M. Auer and J. L. Skinner, “IR and Raman spectra of liquid water: Theory and interpretation,” *J. Chem. Phys.*, vol. 128, no. 22, 2008.

[56] M. Pastorczak, M. Kozanecki, and J. Ulanski, “Raman Resonance Effect in Liquid Water,” *J. Phys. Chem. A*, vol. 112, no. 43, pp. 10705–10707, Oct. 2008.

www.manaraa.com

CHAPTER III

FLUORESCENCE SPECTROSCOPY

3.1 Laser-Induced Fluorescence

When a radiation interacts with certain material, its photons can be either elastically scattered or absorbed depending on whether the photon energy is lower or higher than the band gap of that material respectively. If absorbed, then an electron jumps to a higher energy state from where it can either subsequently fall back to the original valence band state radiatively or decay to slightly lower energy trap state non radiatively. In the latter case, after a short time (to the order of nanoseconds), the electron transits back to the ground state emitting radiation of a lower energy (higher wavelength). This process of emission of photons with higher wavelength is called fluorescence and if induced by laser photons it is called laser-induced fluorescence. Fig 3.1, which is also called as Jablonski diagram, shows the process of fluorescence.

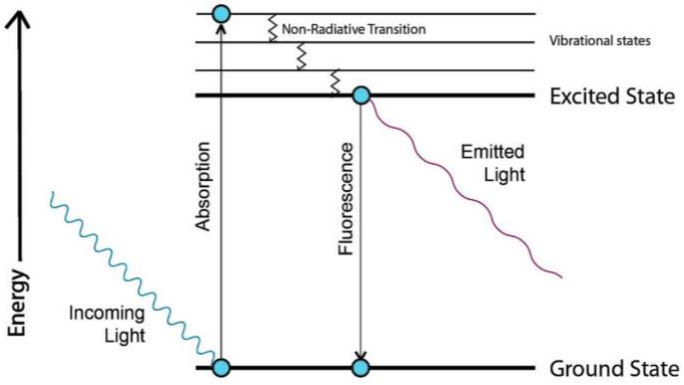

Figure 3.1 Jablonski diagram depicting fluorescence process

www.manaraa.com

Since the emitted radiation is a characteristic of the energy states present in the molecules/ material, it can be used as a tool to identify the specimens. Also due the initial non-radiative decay, the process of fluorescence is independent of the incoming radiation, provided that the incident photons energy is higher than the band gap of the molecules [1].

In vegetation, incident light is absorbed by chlorophyll which uses the energy to drive photosynthesis or is re-emitted in the form of heat or reemission as fluorescence. Chlorophyll fluorescence does not account for a very big percentage of the absorbed light [2] yet has been used for a long time to study physiological changes in plants. The main chlorophyll fluorescence peaks can be found near 690 nm, known as red chlorophyll fluorescence or F690, and 740 nm, known as far-red chlorophyll fluorescence or F740 [3]. While the ratio of F690 and F740 is an excellent indicator of photosynthetic efficiency, there are many factors that can influence photosynthesis and subsequently chlorophyll fluorescence [4]. Other means might have to be employed to confirm the cause of a certain physiological state of a plant, but it can be successfully used as an indicator. There have been many studies correlating changes in chlorophyll fluorescence intensity and the ratio of F690 to F740 to indicate stress of various types [5, 6], fruit ripeness [7, 8], and many others. LIF spectroscopy can also be helpful in identification and quantification of diseases affecting plants [9, 10], such as aflatoxin and various fungal toxins. Aflatoxin is a carcinogenic toxin produced by the *Aspergillus Flavus* fungi which can affect corn, wheat, rice and peanuts among others. The fungal infection *A. Flavus* has been shown to produce fluorescence from UV excitation with a peak around 450 nm [10]. This fluorescence signal is referred to as blue greenish-yellow (BGY).

Polycyclic Aromatic Hydrocarbons (PAHs) are compounds of great environmental interest because of their potential carcinogenic byproducts frequently occurring in the environment [11].

www.manaraa.com

One of the ways these pollutants can enter the environment include petroleum spills and during the incomplete combustion of organic material (petroleum) that is released as smoke by the automobile exhausts. Therefore, it is an important to establish simple, sensitive and reliable methods for the determination of these compounds. Excited at 405 nm, PAH peaks can be observed around 435 nm [12].

A remotely maneuvered aircraft, which can either be controlled from a remote location, or fly completely autonomously according to a pre-planned flight path coupled with a payload falls in the category of UAS (Unmanned Aerial Systems). In the earlier times UAV (Unmanned Aerial Vehicles) or UAS majorly served a purpose only in military use however recently, a number of civilian applications have emerged [13], indicating bright market prospects for the commercial UAVs in the near future. With different types of payloads, UAVs can be tasked for various applications. For example, a NASA Pathfinder Plus UAV is used to capture multispectral imagery over a coffee plantation to further detect ripeness status and evaluate harvest readiness [14, 15]. Using similar approach, this is thesis explains how a UAV can be used to create fluorescence map of a field autonomously.

3.2 Sensor Module Construction

3.2.1 Hardware

The sensor of the LIF module constructed was a micro spectrometer: C12666MA (Hamamatsu Photonics). This micro spectrometer being small size, can easily be integrated into bigger systems. The spectral response of this sensor lies in the visible range (340 - 780 nm) with a maximum resolution of 15 nm passing through 256 bins. A 405 nm diode laser with integrated and variable focusing optics and adjustable power (from 0 – 150 mW) was used as an excitation source in the set-up. A colored glass long pass filter (cut off wavelength: 420nm) was employed

www.manaraa.com

to discard the scattering wavelengths of the incident light in conjunction with a plano-convex lens (NBK-7, Thorlabs) that aided collection of data signals.

The set-up is shown in Fig. 3.2 along with the microcontroller whose function is mentioned below. The optics arrangement thus chosen was economical and extremely modular and versatile. Wider range of targets could be explored by simply changing the laser and its corresponding filter.

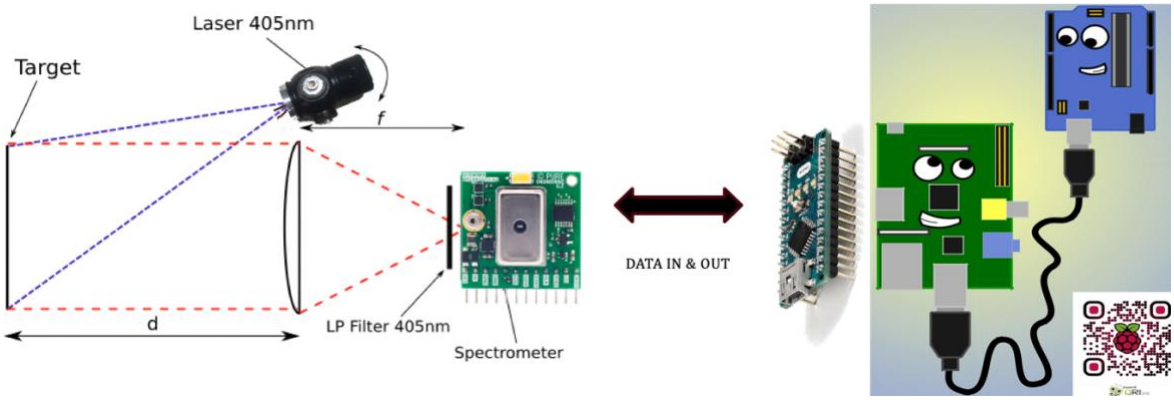

Figure 3.2 (left) Diagram of optics system along with sensor module's interaction with the microcontroller
(right) Higher level communication between RPi and Arduino Nano

In order to store, reference or visualize the date acquired by spectrometer, two unequivocal electronic gears were used. Firstly, a microcontroller (Arduino Nano) which interfaces directly with the spectrometer that has three main functions: to collect spectral responses (by trigger of pin), control parameters (gain and integration time) and store data on the SD card. Secondly, communication and visualization at the higher level was done using a Raspberry Pi, Model 3B (RPi) running on Raspbian operation system using Linux. Interfacing with the RPi was achieved

www.manaraa.com

with a 3-inch touchscreen display. This simplifies the interaction between the user and the sensor module.

Separation in the levels of communication allows for the complete system to be divided into two parts: the sensor and the handheld module enabling the module to be removed from the handheld and integrated into another system easily (explained in section 3.3.4.).

3.2.2 Software

Python, which is an open source programming language, was used as a higher-level software. For a successful communication between the sensor and the RPi, a serial bit transfer protocol was used which could also be utilized for any other device communicating via serial. C language code was used for Arduino Nano to communicate with external devices and spectrometer control. The program to control the spectrometer was adapted directly from Tricorder project and Peter Jansen [19]. The data is read in serial, till end of line (EOL) character or new line ('\n') is reached after which the data is parsed, and response is sent correctly. To develop the user interface, Python and Qt (a cross platform for GUI development) was used with RPI. Thus, the user was able to control the sensor in real time, simultaneously view spectra and change parameters as shown in Fig 3.3.

www.manaraa.com

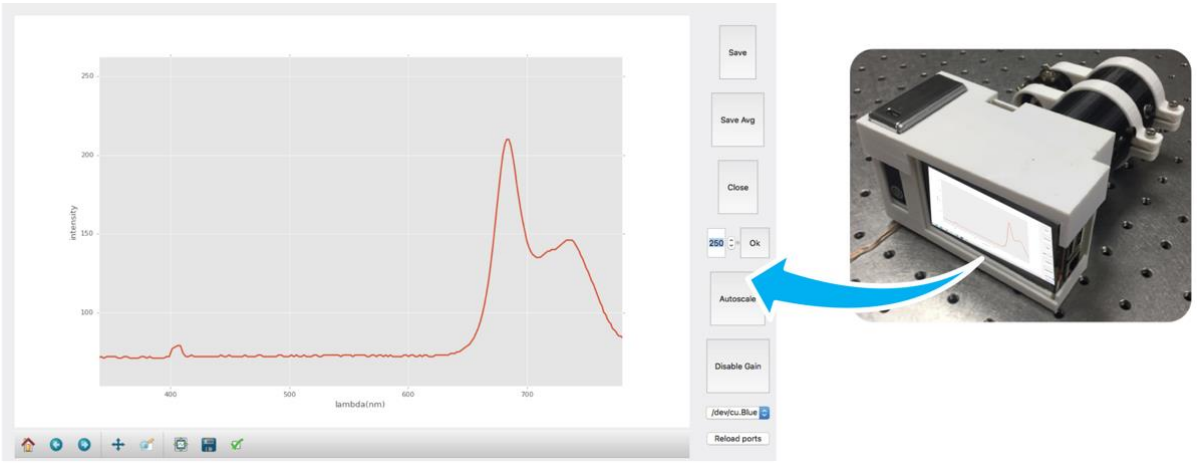

Figure 3.3 (right) The sensor module integrated with the handheld unit and (left) expanded view of the GUI on touch screen

3.2.3 Calibration and Performance Testing

A light source with narrow and well-known spectral lines (a dense helium lamp) [16], was used to calibrate the handheld unit. *MATLAB* was used to fit the calibration data with the reference using quadratic approximation:

$$\lambda(p) = \lambda(0) + C_1 p + C_2 p^2 \tag{3.1}$$

Where,

λ (p) - wavelength of pixel p

λ (0) - is the wavelength at pixel 0

C1 and C2 - coefficients of the fit

www.manaraa.com

The spectral lines of He (from text) and the uncalibrated and calibrated spectrometer spectra of He are shown in Fig. 3.4 and 3.5 respectively.

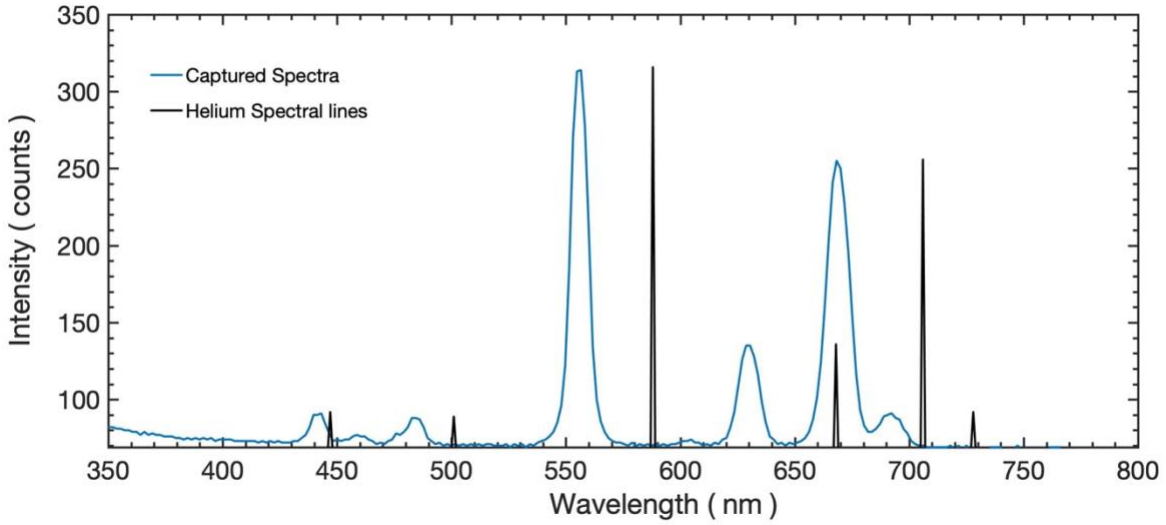

Figure 3.4 Uncalibrated spectrum of a helium lamp (blue) taken from handheld along with known characteristic peaks (black) of helium

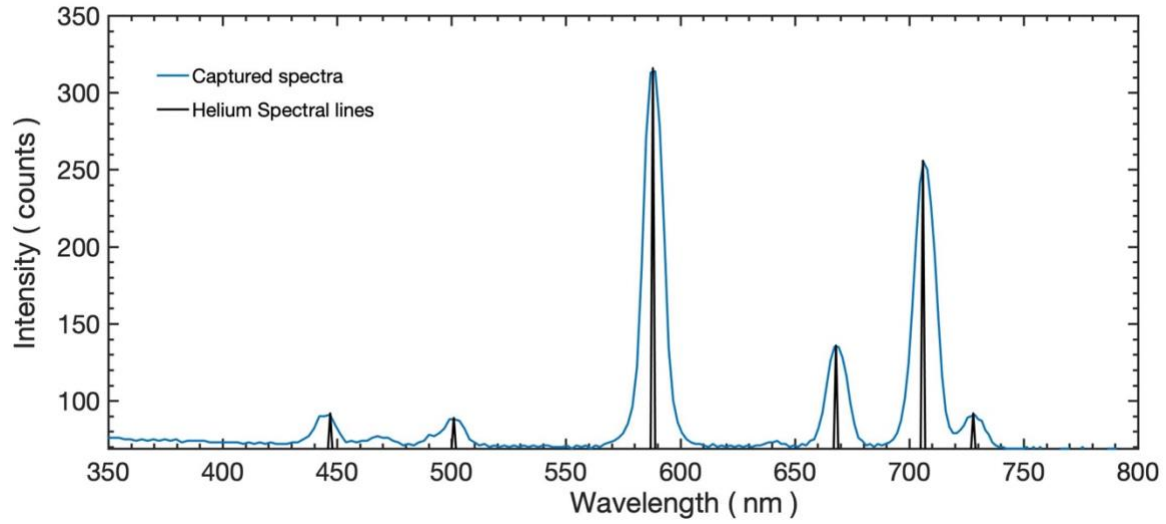

Figure 3.5 Calibrated spectrum of a helium lamp (blue) taken from handheld along with known characteristic peaks (black) of helium

www.manaraa.com

For the purpose of testing this device, chlorophyll spectra from the leaves of an oak tree was taken. It is clear from Fig. 3.6 and Fig. 3.7 that the fluorescence peak intensities at F690 and F740 decreased immensely for the stressed leaves as compared to unstressed leaves. Also, the F690 / F740 ratio changed from 1.55 to 1.15 for stressed and unstressed leaves respectively. Satisfactory results were obtained using integration time of 100ms for a distance of 8m beyond which noise appeared. However, the distance could be extended by increasing the integration time.

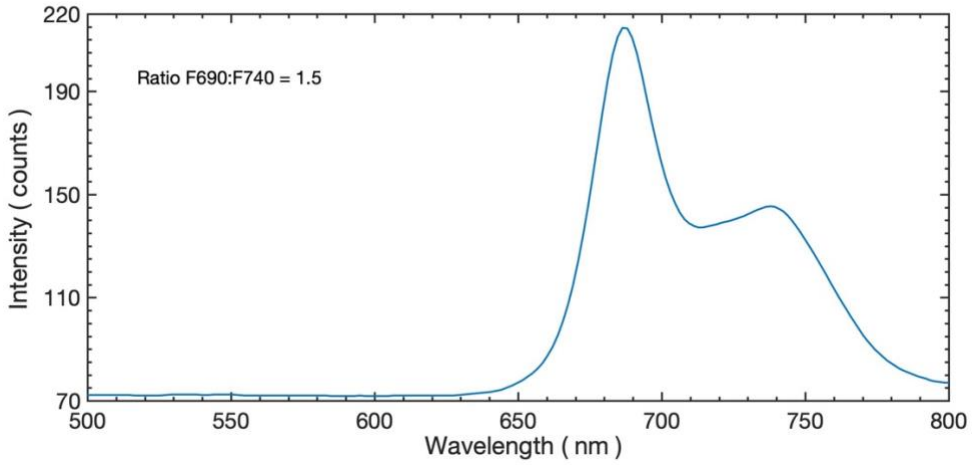

Figure 3.6 Chlorophyll fluorescence spectra of unstressed leaves of water oak tree leaves taken with integration time 100 ms and F690/F740: 1.5

www.manaraa.com

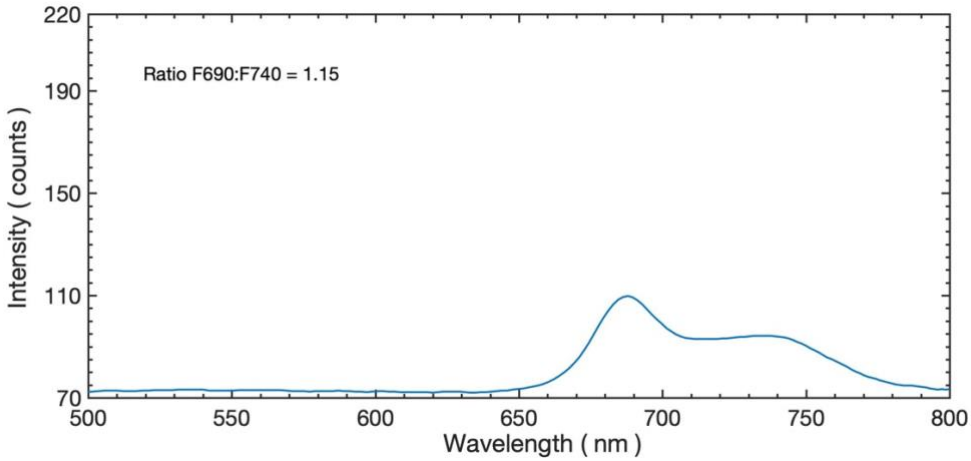

Figure 3.7 Chlorophyll fluorescence spectra of unstressed leaves of water oak tree leaves taken with integration time 100 ms and F69/F740: 1.15

3.2.4 Sample Preparation and Data Acquisition

Chlorophyll fluorescence was measured during the ripening of both granny smith apples (brand name: CMI) and bananas (brand name: Del Monte) purchased from Kroger (fresh food mart). Fluorescence spectra were measured on predetermined spots on apples and bananas using a 405 nm excitation source with laser power 28 mW and integration time set to 200 ms for ten days. The spectra were deconvoluted using constituent peaks (F740 and F690) by the software *OriginLab* and ratios of the peaks were reported.

Samples of corn kernels containing aflatoxin were obtained from department of plant pathology (Mississippi State University) for a test of the aflatoxin detection ability of the portable LIF sensor. Both kernels inoculated with aflatoxin and without inoculation were sampled a several of times using the sensor module. In addition to that, two grades of petrol (high and low grade) were procured from Chevron gas station and fluorescence spectra were measured for both samples using same parameters as were used for fruits.

www.manaraa.com

3.2.5 Results

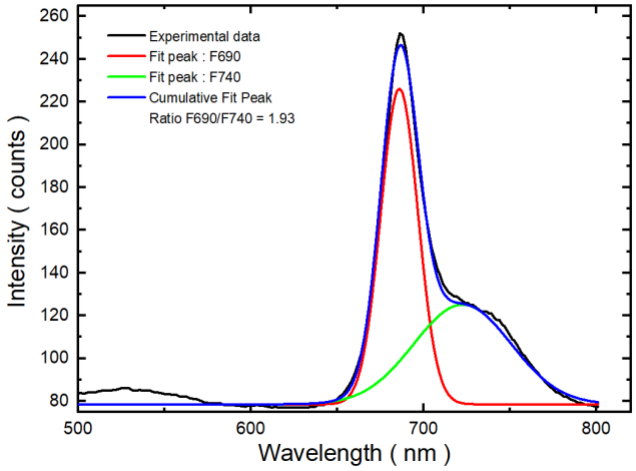

Figure 3.8 Deconvoluted fluorescence spectra of banana on day two and F690/F740 ratio as 1.93

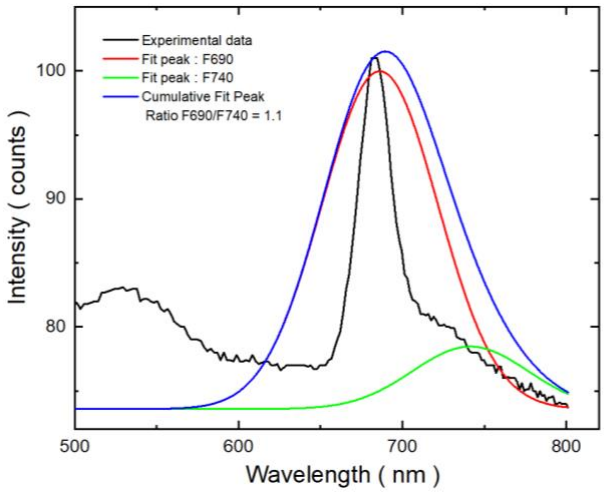

Figure 3.9 Deconvoluted fluorescence spectra of banana on day eight and F690/F740 ratio as 1.1

www.manaraa.com

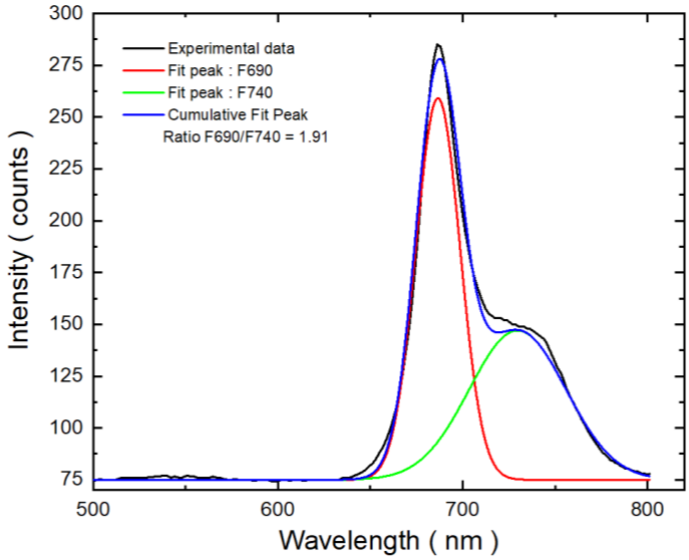

Figure 3.10 Deconvoluted fluorescence spectra of apple on day two and F690/F740 ratio as 1.91

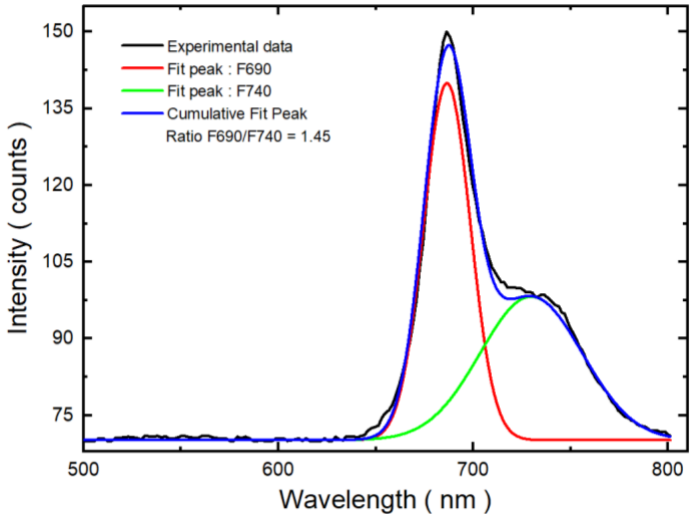

Figure 3.11 Deconvoluted fluorescence spectra of banana on day eight and F690/F740 ratio as 1.45

www.manaraa.com

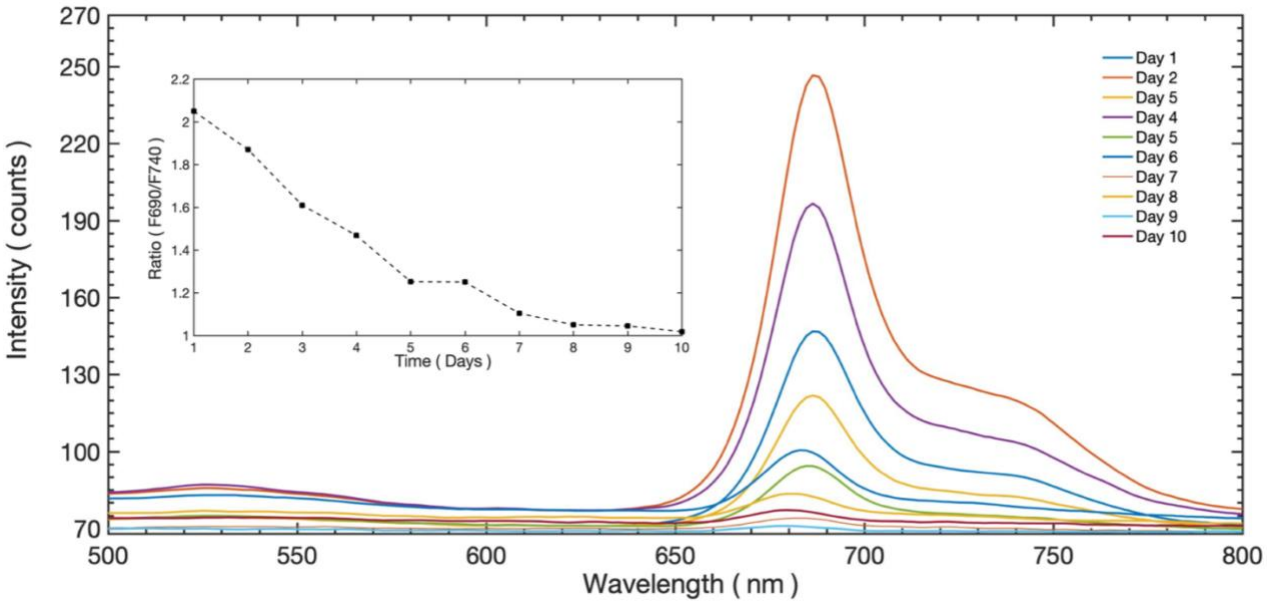

Figure 3.12 Chlorophyll fluorescence of an apple over the course of ten days
F690/F740 ratio plotted against days showing the change in chlorophyll level

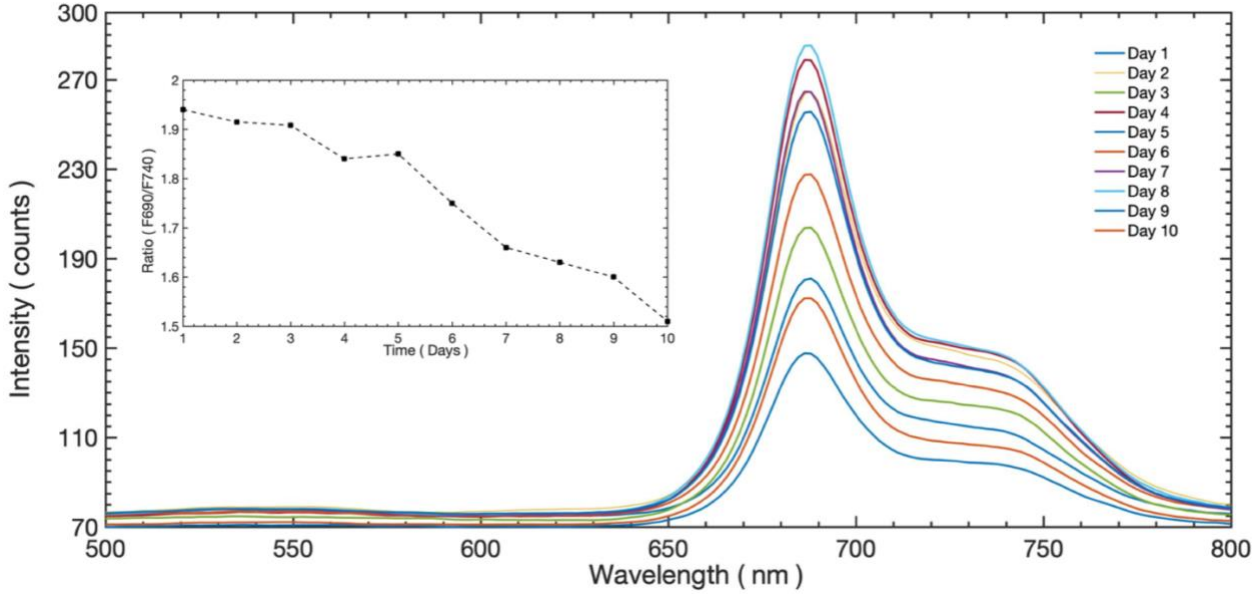

Figure 3.13 Chlorophyll fluorescence of an apple over the course of ten days
F690/F740 ratio plotted against days showing the change in chlorophyll level

www.manaraa.com

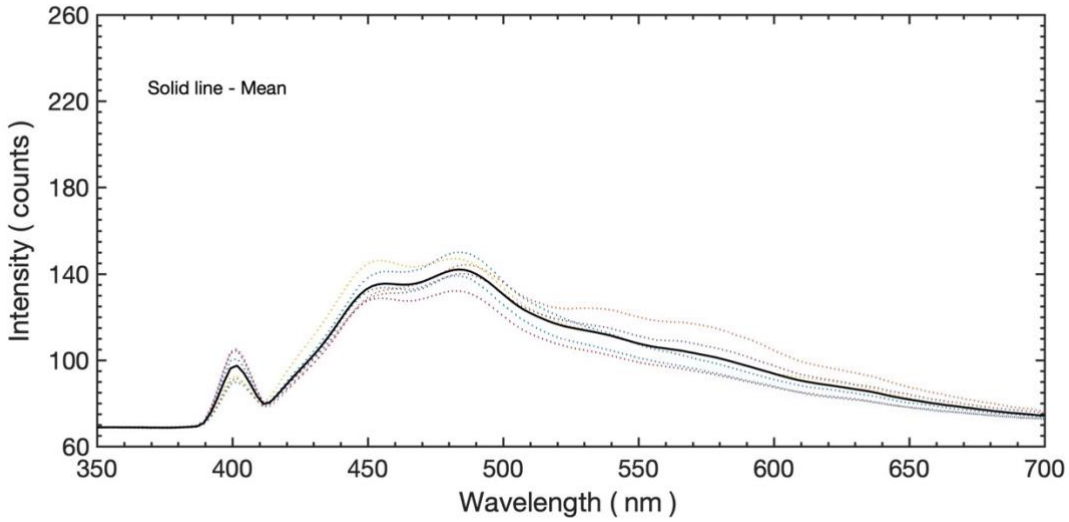

Figure 3.14 Fluorescence spectra collected from kernels with without aflatoxin present in them

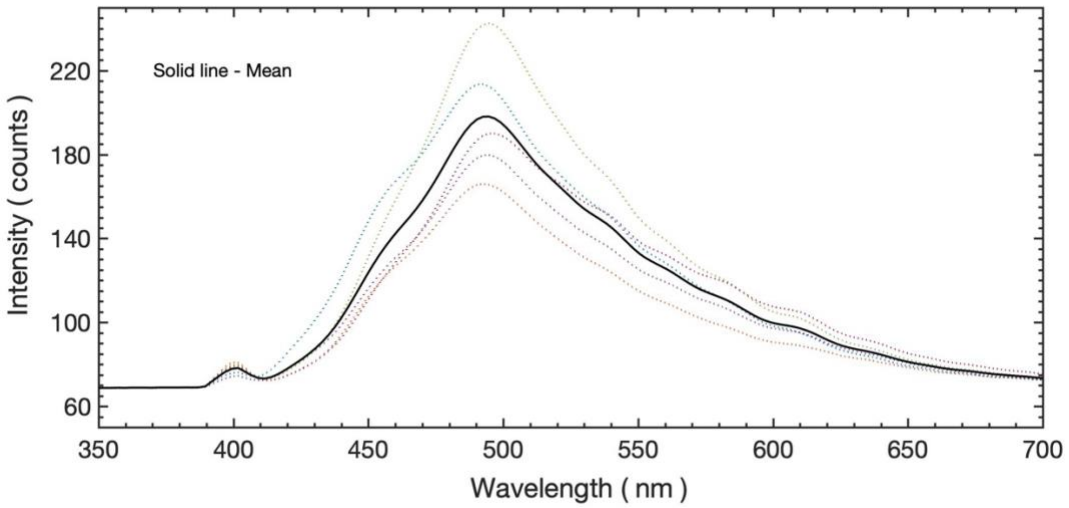

Figure 3.15 Fluorescence spectra collected from kernels with presence of the toxic fungi

www.manaraa.com

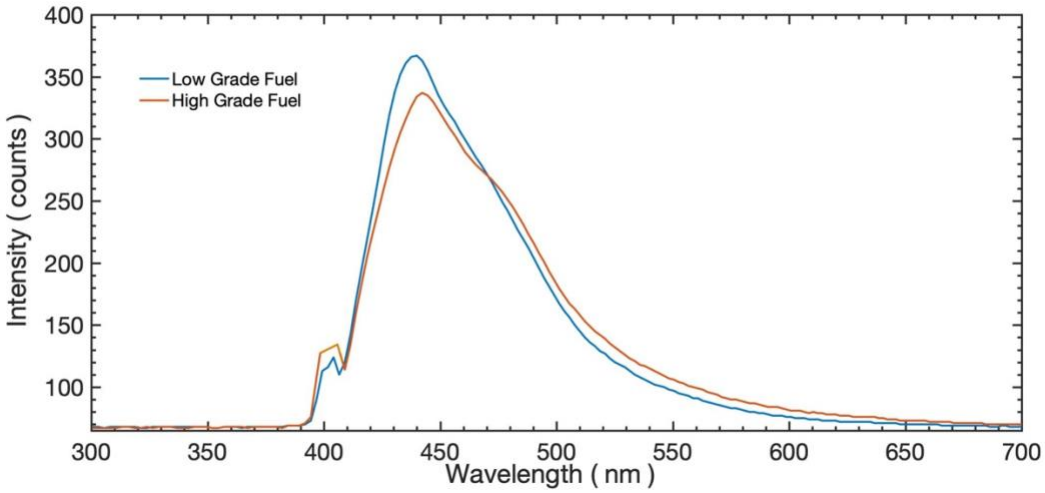

Figure 3.16 Fluorescence spectra collected from two grades (blue: low grade, red: high grade) of petroleum at *Chevron* gas station depicting the presence of PAH levels in both

Figure. 3.8 and 3.9 show the deconvoluted peaks for day two and day eight of chlorophyll peaks: F690 and F740, and their ratios for banana obtained by handheld unit and processed in *OriginLab*. Figure. 3.12 shows the change in fluorescence spectra over 10 consecutive days for a banana and the change in the ratio of F690/F740 peaks are given in the inset. The decrease in the chlorophyll peak intensities prove the fact that fruit ripening occurred during the period of observation. Fig. 3.10 and 3.11 the deconvoluted peaks for day two and day eight of chlorophyll peaks: F690 and F740, and their ratios for apple. Figure. 3.13 shows the chlorophyll fluorescence spectra of apple over the course of ten days and ratio of deconvoluted peaks F690 to F740 vs days on the left. There is decrease in chlorophyll fluorescence as can be seen in the graph for granny smith apple however, the decreasing trend in the F690/F740 ratio, was not as evident as in the bananas. This method of non-invasive ripening detection could be applied towards rapid screening of agronomical procedures. Figure. 3.14 and Fig. 3.15 show a clear difference between the peak intensity of the fungi present in Aflatoxin (*A. Flavus*) between non-infected and infected corn

www.manaraa.com

kernels respectively. These results are consistent with other work showing an increase in BGY fluorescence in the presence of aflatoxin [17]. Detection of this carcinogenic fungus through the integration of the sensor into the UAV that would collect data autonomously is the goal for future. Figure. 3.16 shows noticeable content variation in the PAH levels (peak around 435 nm) in good and bad grade gasoline. While not a rigorous test, it demonstrates the potential ability for this portable device to quickly detect samples with higher PAH content. This can be very useful for laser-induced real time identification of compounds in our surroundings that might emit carcinogenic byproducts due to PAH [18].

www.manaraa.com

3.3 Unmanned Aerial Vehicle

3.3.1 Objective

The goal of this section will be to reconstruct an image of the F690:F740 ratio of a field to map changes in stress among crops being grown. In addition to aerial measurements, the ability for the sensor module to be easily switched into another device allows for follow up measurements in the field. This could help detect disease, infestation, undesirable soil, or poor water. A secondary goal is to have the UAV and sensor module both be as inexpensive as possible while maintaining efficiency.

3.3.2 Construction and Working

For the purpose of remote sensing, a UAV was developed which could carry the sensor unit (payload). The spectrometer module's optics was purposely chosen light weight for easy mounting to the UAV and for higher efficiency. An open source hardware, *APM 2.8* flight controller with an open source software *ArduCopter* were utilized to build and control this UAV. *ArduCopter* firmware and *Mission Planner* application designed for computers can only be used for preloading planned missions onto the controller (*ArduPilot, APM 2.8* in our set-up). There is an additional application for devices with android operating systems by the name of '*Tower*', that allows the quadcopter to be controlled (fed instructions) on site as well and is designed for planning missions for 3D image capture or mapping. *ArduPilot* had an onboard sensor suite including magnetometers that measures magnetic forces, especially the earth's magnetism. This suite also included gyroscopes for angular and linear position, accelerometers for acceleration and speed. To determine the global position and heading a GPS was installed along with a barometer and ultrasonic range finder to determine the height. Complete parameters of height and position etc.

www.manaraa.com

were communicated to the ground station via a radio telemetry link. Thus, our UAV could successfully fly pre planned missions.

3.3.3 Flight Testing

The sensor module was initially mounted to the UAV on a servo-driven gimbal mount which aimed the device directly downward regardless of the UAV's rotation however, the gimbal mount introduced instability of the sensor during flight, hence it was removed and a mount was constructed using 3D printed parts and available laboratory equipment that enabled the sensor module to capture data only when vertically pointed towards at the sample. Several demo missions were created in *Mission Planner* and *Tower*, and the vehicle was flown to test the appropriate speed, altitude and weight of the sensor and mounts. Figure. 3.17 (left) shows the final assembly scheme of the payload (sensor unit) and vehicle that was employed to acquire data.

Figure 3.17 (left) Sensor unit integrated with the UAV using 3D printed and lab made parts. (right) Pictorial demonstration of data collection while in flight

www.manaraa.com

3.3.4 Data Acquisition and Analysis

As described in section 3.3.1, first function of the code on Arduino Nano was that it allowed it to interact with external devices (accept or give commands though I/O pins). Secondary functions included storage of spectrometer data, control of a status LED, and low-level communication via an I/O pin. This last feature allowed the triggering and storage of data by only the changing of one pin with respect to 5V and ground. When the pin was set to ground (on the remote control that interacts with the RC receiver on the quadcopter), data collection began until the pin was set to 5V at which time the data was saved. It had one-way communication with the UAV via the I/O pin. This pin also triggered the sensor module to start collecting data constantly and storing it on an onboard SD card along with a timestamp. The integration time was set to 200 ms before the flight and the vehicle flew at 5 m/s at 10 feet above ground on auto mode where it stopped at ten waypoints as shown (Fig. 3.19 and 3.20) for 20 seconds collected ten data points at each spot triggered via remote. To account for the amount of data saved in flight, a pair of Arduinos Nanos (interreacting through standard serial communication by TX and RX pins) was used. After the mission, the data collected by the sensor module and the data logged by the UAV was coupled and reconstructed into a spectral map showing the data points in the field (Rice field, North farm, Mississippi State University). Due to the way the module was constructed, external light (in this case, sunlight) would have interfered with the fluorescence signal gathered by the sensor, hence all the data acquired was post sunset. The vehicle was always flown in the presence of a certified pilot and with the permission of the faculty. A flow diagram of this control scheme is shown in Fig. 3.18.

www.manaraa.com

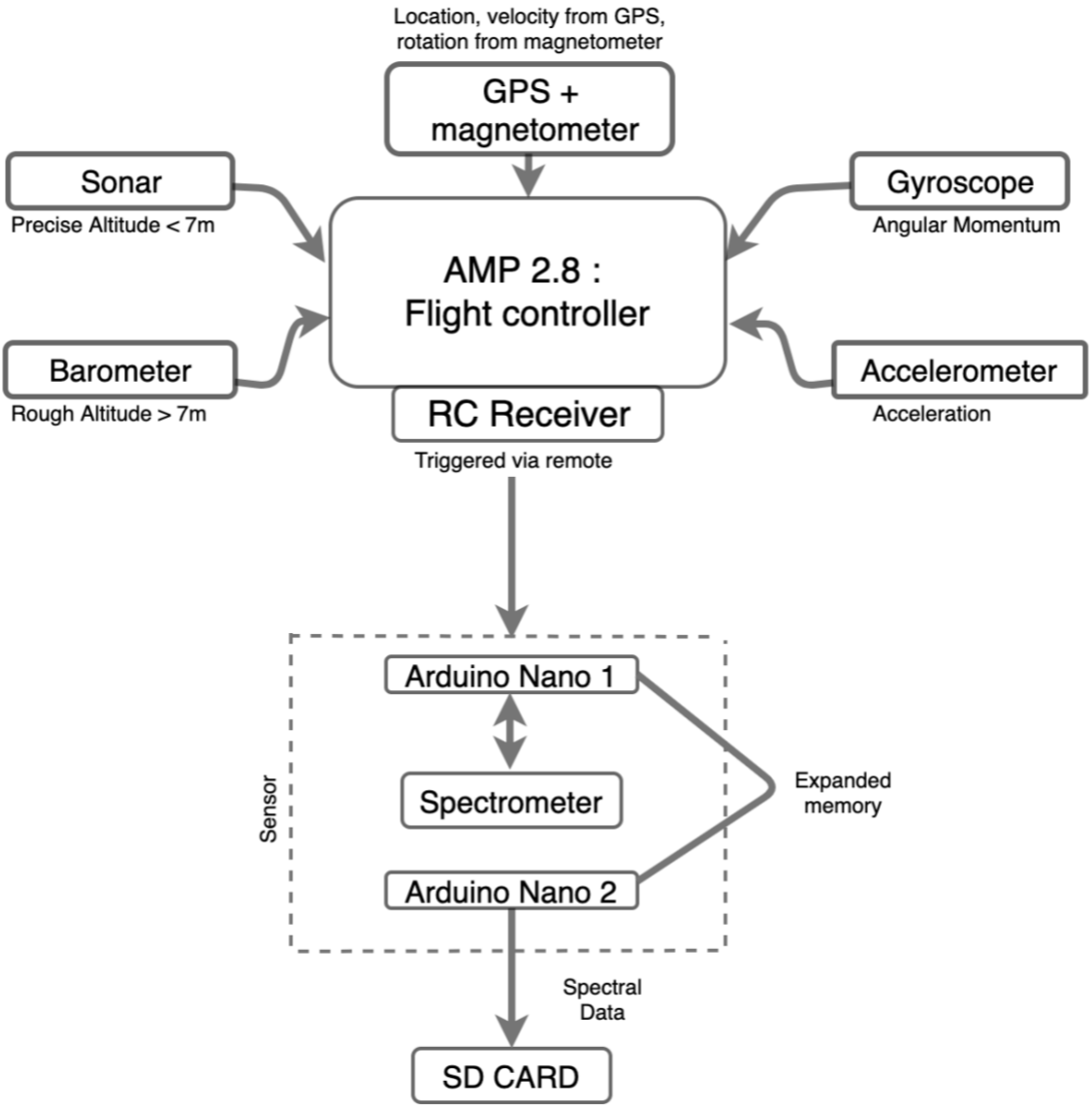

Figure 3.18 Control diagram for the UAV electronics coupled to sensor unit (payload)

www.manaraa.com

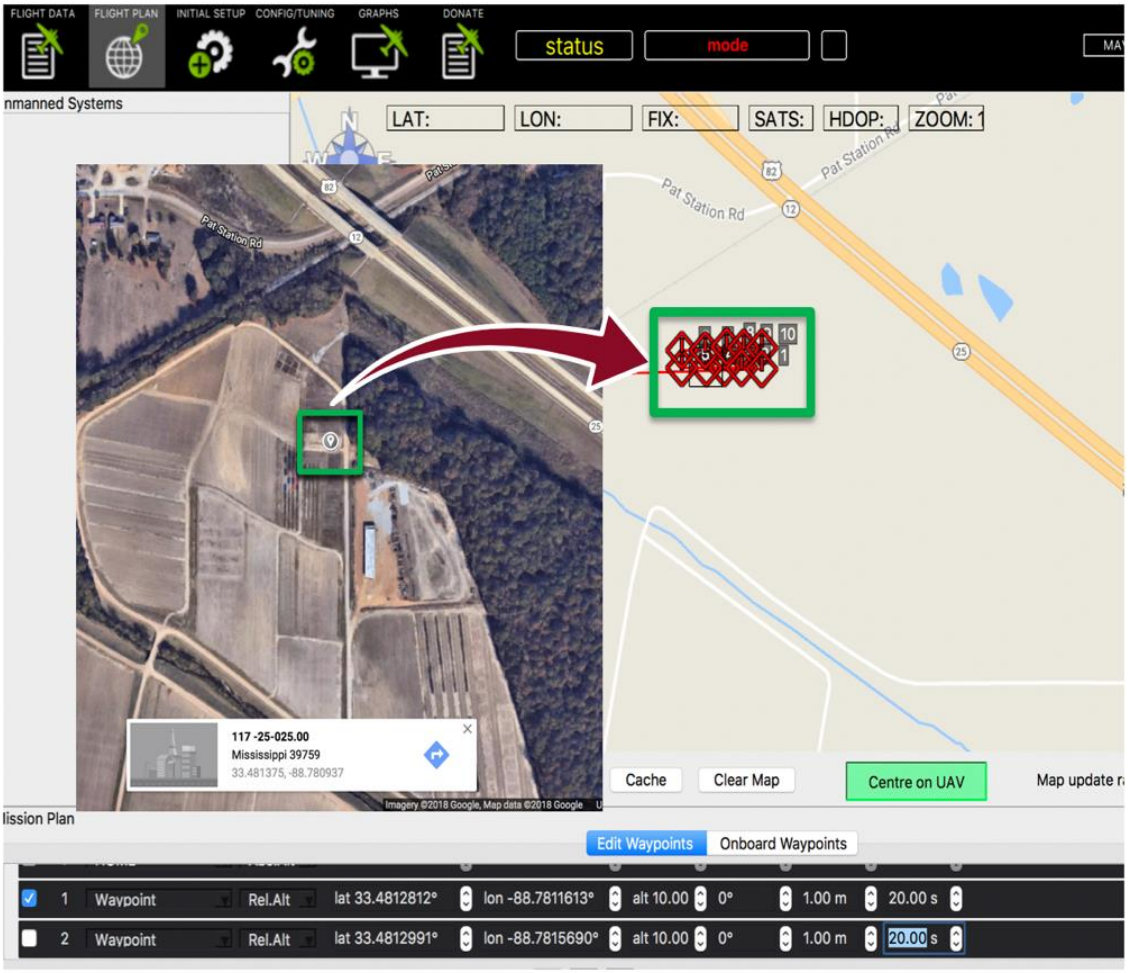

Figure 3.19 Screenshot of Mission planner (*ArduCopter* firmware to plan missions) showing selected data points on the Rice field along with the Google maps screen shot of the same location at Mississippi State university

www.manaraa.com

3.3.5 Results

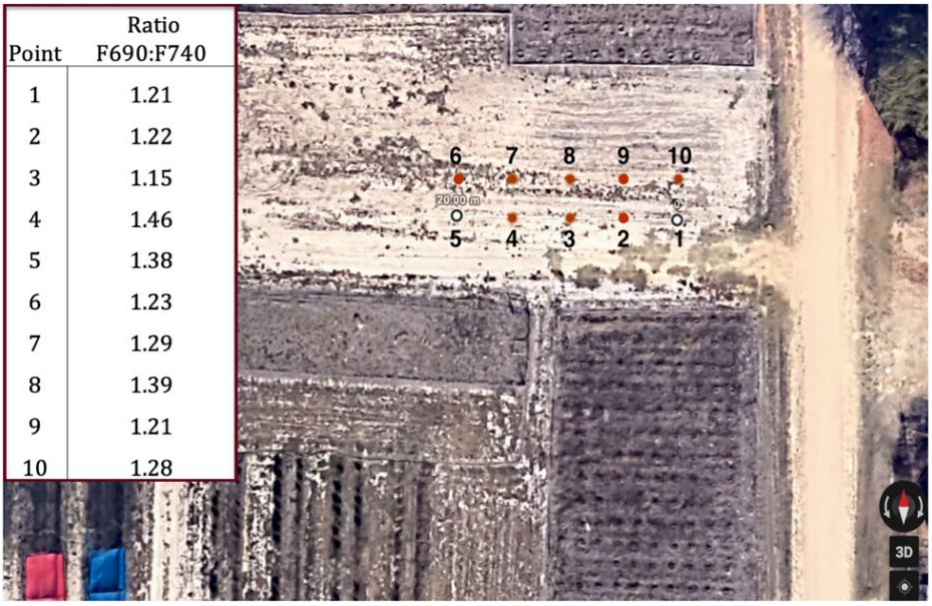

Figure 3.20 Zoomed view of the position of the selected data collection points on the rice field along with the reported data of F690/F740 ratio of the leaves of rice plants at those points

Figure. 3.19 shows a screenshot of the mission uploaded on the firmware along with the position of the target field. The vehicle was successfully able to complete the mission by collecting data on the spots that have been marked over several flights. The F690/F740 ratios of the chlorophyll data of rice plants at early stages were calculated from the acquired spectral data and are shown on the top left of Fig. 3.20, there was no remarkable change in the ratios (F690/F740) of the points shown depicting similar chlorophyll content in those leaves at the time and at the sites data was recorded.

www.manaraa.com

3.3.6 Future Scope

One of the drawbacks of the device in flight is due the angles at which the payload faces vegetation due to either the vehicles rotation or the orientation of the target. It is designed to acquire best data when it is facing the target normally, however in real life situations the locations of targets might not be always perpendicular to the sensor. To improve the scanning, a sturdy gimbal mount can be installed that can change the angles of the sensor, and at the same time does not make the sensor vibrate a lot when acquiring data in flight. Currently the precision of the GPS module installed is about 1 m, however, a better GPS module will be able to distinguish nearby targets, hence would be able to create a more detailed map. This can also be aided by using camera (sensor) calibration in the software.

www.manaraa.com

3.4 References

[1] S. Svanberg, "Fluorescence Spectroscopy and Imaging of Lidar Targets," 2010, pp. 433–467.

[2] K. Maxwell and G. N. Johnson, "Chlorophyll fluorescence - A practical guide," *Journal of Experimental Botany*, vol. 51, no. 345. Oxford University Press, pp. 659–668, 2000.

[3] H. K. Lichtenthaler and J. A. Miehé, "Fluorescence imaging as a diagnostic tool for plant stress," *Trends Plant Sci.*, vol. 2, no. 8, pp. 316–320, Aug. 1997.

[4] Z. G. Cerovic, G. Samson, F. Morales, N. Tremblay, and I. Moya, "Ultraviolet-induced fluorescence for plant monitoring: present state and prospects," *Agronomie*, vol. 19, no. 7, pp. 543–578, 1999.

[5] P. Chen, D. Pan, and Z. Mao, "Development of a portable laser-induced fluorescence system used for in situ measurements of dissolved organic matter," *Opt. Laser Technol.*, vol. 64, pp. 213–219, 2014.

[6] J. Belasque, M. C. G. Gasparoto, and L. G. Marcassa, "Detection of mechanical and disease stresses in citrus plants by fluorescence spectroscopy.," *Appl. Opt.*, vol. 47, no. 11, pp. 1922–6, Apr. 2008.

[7] A. J. Das, A. Wahi, I. Kothari, and R. Raskar, "Ultra-portable, wireless smartphone spectrometer for rapid, non-destructive testing of fruit ripeness," *Sci. Rep.*, vol. 6, Sep. 2016.

[8] I. Urbano Bron, R. Vasconcelos Ribeiro, M. Azzolini, A. Pedro Jacomino, and E. Caruso MacHado, "Chlorophyll fluorescence as a tool to evaluate the ripening of 'Golden' papaya fruit," *Postharvest Biol. Technol.*, vol. 33, no. 2, pp. 163–173, Aug. 2004.

[9] E. C. Lins, J. Belasque, and L. G. Marcassa, "Detection of citrus canker in citrus plants using laser induced fluorescence spectroscopy," in *Precision Agriculture*, 2009, vol. 10, no. 4, pp. 319–330.

[10] M. C. Rodríguez, G. H. Sánchez, M. S. Sobrero, A. V. Schenone, and N. R. Marsili, "Determination of mycotoxins (aflatoxins and ochratoxin A) using fluorescence emission-excitation matrices and multivariate calibration," *Microchem. J.*, vol. 110, pp. 480–484, Sep. 2013.

[11] H. I. Abdel-Shafy and M. S. M. Mansour, "A review on polycyclic aromatic hydrocarbons: Source, environmental impact, effect on human health and remediation," *Egyptian Journal of Petroleum*, vol. 25, no. 1. Egyptian Petroleum Research Institute, pp. 107–123, 01-Mar-2016.

[12] T. L. Yeo, K. B. Ozanyan, F. Hindle, N. R. J. Poolton, and H. McCann, "Characteristics of gasoline fluorescence using 404-nm semi-conductor laser diode excitation," *Appl. Spectrosc.*, vol. 56, no. 7, pp. 846–851, Jul. 2002.

[13] H. Chao, Y. Cao, and Y. Q. Chen, "Autopilots for small fixed-wing unmanned air vehicles: A survey," in *Proceedings of the 2007 IEEE International Conference on Mechatronics and Automation, ICMA 2007*, 2007, pp. 3144–3149.

www.manaraa.com

[14] L. F. Johnson, S. R. Herwitz, B. M. Lobitz, and S. E. Dunagan, "Feasibility of monitoring coffee field ripeness with airborne multispectral imagery," *Appl. Eng. Agric.*, vol. 20, no. 6, pp. 845–849, Oct. 2013.

[15] S. R. Herwitz *et al.*, "Imaging from an unmanned aerial vehicle: Agricultural surveillance and decision support," *Comput. Electron. Agric.*, vol. 44, no. 1, pp. 49–61, Jul. 2004.

[16] N. Abramzon and P. B. Siegel, "Introductory helium atomic spectrum analysis," *Am. J. Phys.*, vol. 77, no. 10, pp. 920–922, Sep. 2009.

[17] H. Yao, Z. Hruska, R. Kincaid, R. Brown, T. Cleveland, and D. Bhatnagar, "Correlation and classification of single kernel fluorescence hyperspectral data with aflatoxin concentration in corn kernels inoculated with Aspergillus flavus spores," *Food Addit. Contam. - Part A Chem. Anal. Control. Expo. Risk Assess.*, vol. 27, no. 5, pp. 701–709, May 2010.

[18] D. M. and M. O., "Polycyclic Aromatic Hydrocarbons a Constituent of Petroleum: Presence and Influence in the Aquatic Environment," in *Hydrocarbon*, InTech, 2013.

[19] P. Jansen, https://www.tricorderproject.org.

www.manaraa.com